REPORT DOCUMENTATION PAGE

Form Approved OMB No. 0704-0188

1. REPORT DATE *(DD-MM-YYYY)*	2. REPORT TYPE	3. DATES COVERED *(From – To)*
26-10-2009	Final Report	15 Oct 2008 – 14 Oct 2009

4. TITLE AND SUBTITLE

Scaled-Up Nonequilibrium Air Plasmas

5a. CONTRACT NUMBER
FA8655-08-1-3061

5b. GRANT NUMBER

5c. PROGRAM ELEMENT NUMBER

6. AUTHOR(S)

Dr. Zdenko Machala

5d. PROJECT NUMBER

5d. TASK NUMBER

5e. WORK UNIT NUMBER

7. PERFORMING ORGANIZATION NAME(S) AND ADDRESS(ES)
Comenius University
FMFI UK
Bratislava 84248
SLOVAKIA

8. PERFORMING ORGANIZATION REPORT NUMBER

N/A

9. SPONSORING/MONITORING AGENCY NAME(S) AND ADDRESS(ES)

EOARD
Unit 4515 BOX 14
APO AE 09421

10. SPONSOR/MONITOR'S ACRONYM(S)

11. SPONSOR/MONITOR'S REPORT NUMBER(S)
Grant 08-3061

12. DISTRIBUTION/AVAILABILITY STATEMENT

Approved for public release; distribution is unlimited.

13. SUPPLEMENTARY NOTES

14. ABSTRACT

This report results from a contract tasking Comenius University as follows: In the first stage of the project we will design a new discharge chamber allowing investigations of the proposed DC discharges in atmospheric pressure steady-state or fast flow conditions, and in lowered pressure. Fast flow conditions will be provided by a special nozzle. The chamber will be optionally mounted on the existing 3 kW microwave plasma torch to investigate discharges in preheated gas flows. The discharge chamber will enable the electrical, optical and spectroscopic diagnostics of the discharges. The measured discharge parameters will allow us to calculate and estimate further properties of the generated non-thermal plasmas. The high voltage generators and the electrical circuits for sustaining optimal discharge regimes have already been constructed.

The main stage of the project will be dedicated to the investigations of the discharge properties in various flow, pressure (1 to 0.1 atm) and temperature (ambient vs. preheated to 2000 K) conditions. The two principal objectives will be sought: volume scaling-up and power budget reduction. Both DC glow and pulsed transient spark discharges will be investigated. Various electrode arrangements with several electrode pairs will be tested to increase the plasma volume. In addition, thermionic cathodes (LaCrO3, LaB6) will be examined to enhance the electron number density in the plasma – a key parameter for plasma shielding. In reducing the power budget we will focus on 1) shortening the transient spark pulses that will reduce the energy losses for gas heating, and 2) increasing the pulse repetitive frequency to keep the electron density large enough (>10e12 cm-3) during the relaxation phase between the consecutive pulses.

The electrical characteristics of the discharges will be measured by using available high voltage probes Tektronix and North Star, and Rogowski current monitor Pearson Electronics altered with a 50 Ohm or 1 Ohm resistor shunt. Both voltage and current signals will be recorded by the digitizing 200 MHz oscilloscope Tektronix TDS 2014 and computer processed. The gas flow conditions will controled with flow meters Aalborg. By changing the gap distance, we will investigate the features of particular discharge zones and measure the cathode fall in the glow discharge regime. Current density, electric field strength and other important plasma parameters will be calculated.

Optical emission spectroscopy is known to be a very useful diagnostic technique of plasmas because it allows identification of active species and radicals in the plasma; measuring the gas temperature (as the rotational temperature that equilibrates with the gas temperature owing to fast collisional relaxation at atmospheric pressure); determining the level of nonequilibrium (by comparing rotational and vibrational temperatures), and under certain assumptions measuring the discharge dimensions. The emission spectroscopy optical system will be constructed using a dual fiber-optic compact spectrometer Ocean Optics SD2000 with CCD detector for fast but low resolution scanning in the UV and VIS-NIR regions (200-500 and 500-1050 nm). Alternatively, for much better spectral and temporal resolution necessary to track the nanosecond-short time scale processes occurring in the transient spark pulses, we plan to use an existing 2-m monochromator Carl Zeiss Jena PGS2 covering UV and VIS (200-800 nm) and providing spectral resolution of 0.05 nm. This will be equipped with a planned intensified CCD camera for ns temporal resolution. The optical system will also comprise filters, lenses, spherical mirrors, irises, pinholes, and fiber

optics. The system will be aligned and focused by a He-Ne laser, and calibrated with optical standards (tungsten and deuterium lamps) borrowed from our international partner, Prof. Christophe O. Laux from Ecole Centrale Paris, France. Measurements of the rotational and vibrational temperatures will be performed by comparing the experimental and the simulated spectra. For spectral simulations, we will use the SPECAIR code developed by C. Laux as well,. Measured temperatures will allow us determining gas temperature, thermal nonequilibrium, and together with electrical discharge characteristics, estimating the electron density and reduced electric field strength (E/N). Emission spectra will be also used to identify the active species and to measure the discharge dimensions. In addition to emission spectroscopy, a digital camera with a few wavelength-specific optical filters will be used for photo-documentation of the discharges to observe their general character and to measure their diameters.

Personnel
Principal investigator: Zdenko Machala, PhD.
- PhDs 2000 Univ. Paris XI, France, and 2001 Comenius Univ. Bratislava, Slovakia
- Post-doc 2002-2004 Stanford Univ., USA
- Currently assistant professor at Comenius Univ. Bratislava, Slovakia
- PI of one national and one international (NATO) grant
- Vice-PI of three other national grants
- Supervising 1 PhD and 2 MSc students
- 7 CC journal publications, 28 conference contributions and other publications,
- 13 SCI citations, 11 other citations
- Research expertise: physics of atmospheric electrical discharges, optical emission spectroscopy, FTIR spectroscopy, plasma chemistry
- Teaching 6 courses in environmental physics

Vice-principal investigator: Karol Hensel, PhD.
- PhD 2002 Saga Univ., Japan
- Post-doc 2002-2003 Toyohashi Univ. of Technology, Japan
- Currently assistant professor at Comenius Univ. Bratislava, Slovakia
- PI of four national grants and one international grant
- Vice-PI of one national and one international grant
- Supervising 1 MSc student
- 9 CC journal publications, 48 conference contributions and other publications,
- 11 SCI citations, 15 other citations
- Research expertise: physics of atmospheric electrical discharges, FTIR spectroscopy, plasma chemistry and catalysis, environmental pollution
- Teaching 5 courses in environmental physics

Other personnel:
Mario Janda, PhD. (post-doc)
Igor Jedlovsky, MSc. (PhD student)
2-3 MSc students
Prof. Christophe O. Laux, PhD., Ecole Centrale Paris, France (consultant)
Dr. Emmanuel Marode, Univ. Paris XI, France (consultant)

Schedule of reports
One annual report will be delivered at the end of the contract.

15. SUBJECT TERMS
EOARD, Plasma Physics

16. SECURITY CLASSIFICATION OF:			**17. LIMITATION OF ABSTRACT**	**18, NUMBER OF PAGES**	**19a. NAME OF RESPONSIBLE PERSON**
a. REPORT	**b. ABSTRACT**	**c. THIS PAGE**			SURYA SURAMPUDI
UNCLAS	UNCLAS	UNCLAS	UL	40	**19b. TELEPHONE NUMBER** *(Include area code)* +44 (0)1895 616021

SCALED-UP NONEQUILIBRIUM AIR PLASMAS

Comprehensive Final Report
for the period: 15 October 2008 – 14 October 2009

Submitted to
Dr. Surya Surampudi
European Office of Aerospace Research and Development
Air Force Office of Scientific Research

Grant No. FA8655-08-1-3061

Submitted by
Professor Zdenko Machala (Principal Investigator)
Department of Astronomy, Earth Physics and Meteorology
Faculty of Mathematics, Physics and Informatics, Comenius University
Mlynska dolina F2, 84248 Bratislava, Slovakia
tel: +421-2-60295618, fax: +421-2-65425982
email: machala@fmph.uniba.sk
http://enviro.fmph.uniba.sk/machala

October 2009

Contents

List of Figures

1. Abstract

The objective of the current program is to investigate the volume scalability of nonequilibrium plasmas produced by electrical discharges in atmospheric pressure air. Both DC and repetitively pulsed discharges have been successfully demonstrated to form non-equilibrium air plasmas at atmospheric pressure with temperatures below 2000 K and electron densities above 10^{12} cm^{-3}. Such plasmas represent a potential for aircraft shielding, and many other applications, e.g. bio-decontamination. The critical issues are the dimensions of these plasma discharges that are typically limited to cm-lengths and mm-diameters at maximum, and the power requirements.

Key results demonstrate that both DC glow discharge and pulsed transient spark generate air plasmas of required parameters. Glow discharge is easier for volume scaling but requires larger power. Glow discharge operated in fast air flows preheated to 2000 K improves the volume scaling but at very high powers (including the preheating). The preheated air can be set below 2000 K at slower flows, thus enabling partial gas heating of the discharge. Corona as a temperature probe was developed to diagnose the microwave preheated air.

A new concept of the DC-driven pulsed discharge was tested: *transient spark*, a repetitive streamer-to-spark transition discharge regime of very short pulse duration (~10-100 ns) and with a very limited energy so that the generated plasma is highly nonequilibrium. This discharge can be maintained at low energy conditions by an appropriate choice of the resistances and capacities in the electrical circuit, and its frequency can be controlled by the applied voltage. Its activity is comparable with the nanosecond repetitive pulsed discharges but its advantage is an ease of the DC operation and no need of special and expensive high voltage pulsers with high repetitive frequency and nanosecond rise-times. Our calculations of temporal evolution of electron density in transient spark show that ~10^{16} cm^{-3} at maximum and ~10^{11} cm^{-3} in average are reached.

Optical emission spectroscopy combined with electrical measurements are used as principal discharge diagnostics techniques.

2. Introduction

This interim report describes progress on our research program "Scaled-up Nonequilibrium Air Plasmas." This program is supported by a grant from the European Office of Aerospace Research and Development of Air Force Office of Scientific Research (Grant No. FA8655-08-1-3061) and is conducted in the group of Prof. Zdenko Machala at Comenius University in Bratislava. This research program follows up the results obtained by the Stanford Consortium of the Plasma Rampart MURI program (Mechanisms of Ionizational Nonequilibrium in Air Plasmas, 1997-2002), and by the Stanford University program (Scaled-Up Nonequilibrium Air Plasmas, 2001-2004), both financed by AFOSR. Prof. Zdenko Machala was personally involved in these Stanford programs in 2002-2004.

Large-volume air plasmas at atmospheric pressure present considerable interest for a wide range of Air Force applications in plasma aerodynamics and flow control. Desirable conditions are electron densities of the order of 10^{12} cm^{-3} and gas temperatures less than 2000 K. Considerable advances have been achieved in the preceding AFOSR programs (MURI program on Air Plasma Ramparts [1] and Scaled-Up Air Plasmas [2]). In particular, they have demonstrated that it is possible to produce over 10^{12} electrons/cm^3 in atmospheric pressure air with either DC or repetitively pulsed discharges. Furthermore, they have experimentally demonstrated that it takes only 12 W/cm^3 of power to produce 10^{12} electrons/cm^3 with a repetitively pulsed discharge in air. This power level is about 250 times lower than for a DC discharge producing the same electron density.

The present program seeks to expand on the results of these preceding programs. Specifically, we are interested in scaling up the DC discharges to produce larger volumes of nonequilibrium air plasma and to reduce the power budget. At the same time we make efforts to understand the elementary processes and their temporal evolution and the physical mechanisms that limit the size of an individual discharge

Section 3 provides an overview of our experimental setups and describes the diagnostics methods used. Section 4.1 describes various DC discharge regimes and their transitions: from streamers to spark to glow discharge. Section 4.2 is devoted to experimental results with DC glow discharges in ambient atmospheric pressure air, including the results of the emission spectroscopy, temperature measurements and radical concentration measurements. Section 4.3 presents some experimental results on DC glow discharges in microwave preheated air flows. Section 4.4 is focused on our most recent results of experiments with transient spark, detailing the electrical and optical characteristics of this spontaneously pulsing discharge providing highly nonequilibrium air plasma at relatively low power requirements and showing the calculation of the electron density.

3. Experimental setup and methods

3.1. Electrical circuit

Atmospheric pressure DC discharges are obtained by applying a few kilovolts between ballasted electrodes. A home-made 25 kV DC power supply is employed, together with a ballast resistor of 0.8-20 MΩ in series with the discharge, as shown in Figure 1. The appropriate value of the ballast resistor is chosen according to the discharge regime and operating current in order to stabilize the discharge.

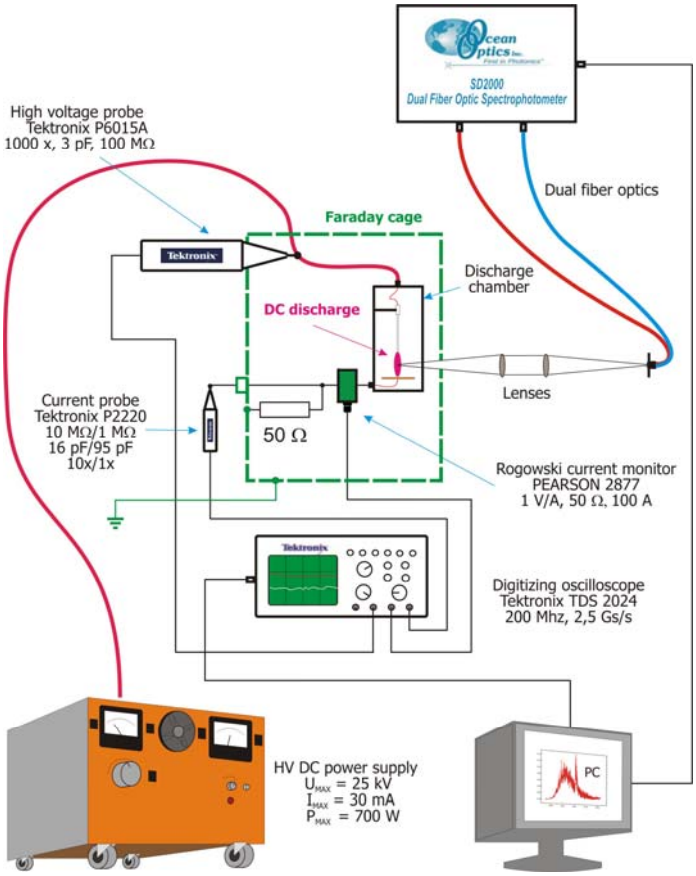

Figure 1. Overall view of the experimental setup for the DC discharges.

The DC discharges are typically applied between stainless steel needle and copper plane or between two platinum pins parallel or perpendicular to the axis of the air flow. The pins are welded onto cooled stainless steel tubes in order to prevent their melting at the elevated temperature operation. In case of the plane cathode, this can be submerged in water, which simulates water treatment or bio-decontamination without significantly influencing the discharge parameters.

In the first stage of the project we designed a new discharge chamber allowing investigations of the proposed DC discharges in atmospheric pressure steady-state or fast flow conditions, and in lowered pressure (Figure 2). The DC discharges can be optionally run in the plasma plume of the 3 kW microwave plasma torch (Litmas Red) to investigate discharges in preheated gas flows. The experimental setup enables the electrical, optical and spectroscopic diagnostics of the discharges. The measured discharge parameters allow us to calculate and estimate further properties of the generated non-thermal plasmas.

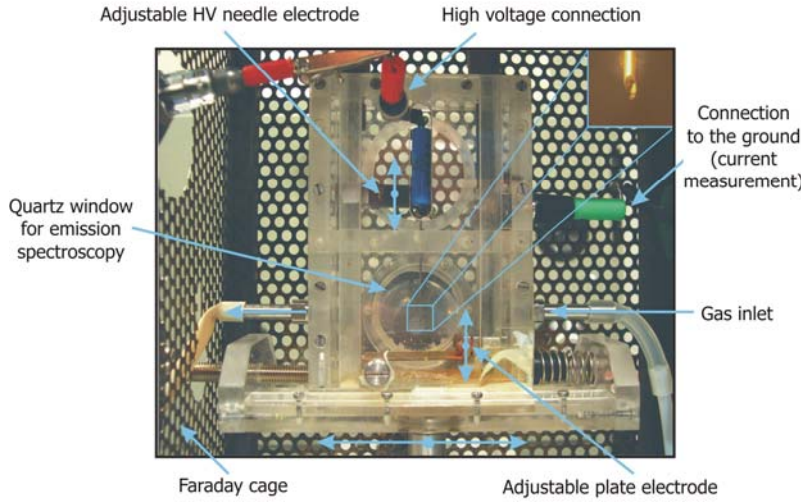

Figure 2. Discharge chamber for electrical and optical investigations of the DC discharges in atmospheric pressure steady-state or fast flow conditions.

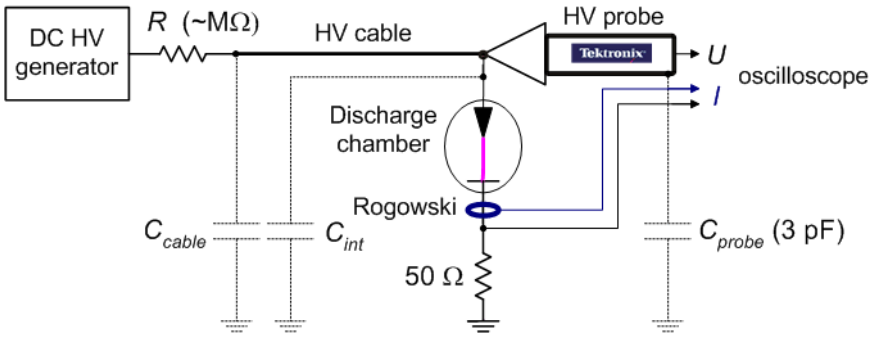

Figure 3. Schematic of the electrical circuit of the DC discharges.

A simplified electrical scheme is depicted in Figure 3. The electrical characteristics of the discharges are measured by using high voltage probes Tektronix and North Star, and Rogowski current monitor Pearson Electronics altered with a 50 Ω or 1 Ω resistor shunt. Both voltage and current signals are recorded by the 200 MHz digitizing oscilloscope Tektronix TDS 2024 and computer-processed. The gas flow conditions are controlled with flow meters Aalborg. By changing the gap distance, we investigate the features of particular discharge zones and measure the cathode fall in the glow discharge regime. Current density, electric field strength and other important plasma parameters are then calculated.

3.2. Optical Diagnostics

Optical emission spectroscopy (OES) is known to be a very useful diagnostic technique of plasmas because it allows identification of active species and radicals in the plasma; measuring the gas temperature (as the rotational temperature T_r that equilibrates with the gas temperature owing to fast collisional relaxation at atmospheric pressure); determining the level of nonequilibrium (by comparing rotational and vibrational T_v temperatures), and under certain assumptions measuring the discharge dimensions. Spectra of the 2nd and 1st positive systems of N_2 ($C^3\Pi_u$-$B^3\Pi_g$ and $B^3\Pi_g$-$A^3\Sigma_u^+$), in some cases also 1st negative system of N_2^+ ($B^2\Sigma_u^+$- $X^2\Sigma_g^+$), NO γ system ($A^2\Sigma^+$-$X^2\Pi_r$), and OH system ($A^2\Sigma^+$-$X^2\Pi_{3/2}$) were used to determine these plasma parameters.

The emission spectroscopy optical system is constructed using a dual fiber-optic compact spectrometer Ocean Optics SD2000 with CCD detector for fast but low resolution scanning in the UV and VIS-NIR regions (200-500 and 500-1050 nm). Alternatively, for much better spectral and temporal resolution necessary to track the nanosecond-short time scale processes occurring in the transient spark pulses, we started using a 2-m monochromator Carl Zeiss Jena PGS2 covering UV and VIS (200-800 nm) and providing spectral resolution of 0.05 nm. This is equipped with a recently bought intensified CCD camera Andor Istar for nanosecond temporal resolution. The optical system also comprises filters, off-axis parabolic and planar mirrors, irises, pinholes, and fiber optics. The discharge chamber and the optical components are mounted on translation stages, which enable lateral and vertical scanning capabilities.

The system is aligned and focused by a He-Ne laser, and calibrated with optical standards (tungsten and deuterium lamps traceable to NIST standards) borrowed from our international partner, Prof. Christophe O. Laux from Ecole Centrale Paris, France. Measurements of the rotational and vibrational temperatures are performed by comparing the experimental and the simulated spectra. For spectral simulations, we use the SPECAIR code developed by C.O. Laux as well [3]. Measured temperatures allow us determining gas temperature, thermal non-equilibrium, and together with electrical discharge characteristics, estimating the electron density and reduced electric field strength (*E/N*). Emission spectra are also used to identify the active species and to measure the discharge dimensions. In addition to emission spectroscopy, a digital camera Olympus E400 with a few wavelength-specific optical filters is used for photo-documentation of the discharges to observe their general character and to measure their diameters.

Transient spark was also investigated in Ecole Centrale Paris together with Prof. C.O. Laux. There, the UV-VIS spectra were obtained using a monochromator Acton SpectraPro 2500i fitted with an intensified CCD camera Princeton Instruments PI-MAX. For time-resolved optical emission measurements, a photomultiplier tube (PMT) module with a 1.4-ns rise time (Hamamatsu H9305-3) was used in place of the monochromator. Its signal was recorded using the oscilloscope. Whenever it was necessary to isolate a specific spectral transition for PMT measurements, a bandpass interference filter (e.g. Melles Griot 03 FIU 127 for the N_2 C-B 0-0 transition) was inserted into the optical path. This experimental set-up is depicted in Figure 4.

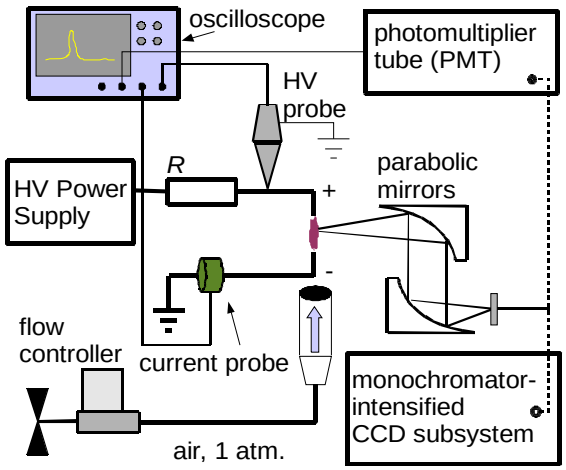

Figure 4. Schematic of the experimental set-up and optical diagnostics used in Ecole Centrale Paris, R - resistor.

3.3. Microwave Plasma Torch

Experiments with DC discharges were planned in ambient and preheated air at atmospheric pressure. We preheat air to about 2000 K with a microwave plasma torch Litmas Red powered by a 5 kW magnetron Richardson Electronics switching power generator Model SM1050. The torch has a maximum power output of 3 kW. The temperature and velocity of the outgoing plasma can be set by varying the power output and gas flow rate, as well as by using water-cooled test sections and nozzles. The torch is able to generate air plasmas in the temperature range 750-4700 K at flow velocities from 20 to 1400 m/s, corresponding to gas flow rates from 8 to 110 slpm (standard liters per minute). The microwave torch head and a close-up view of the air plasma plume at typical experimental conditions (T~2000 K, v~1000 m/s) are shown in Figure 5.

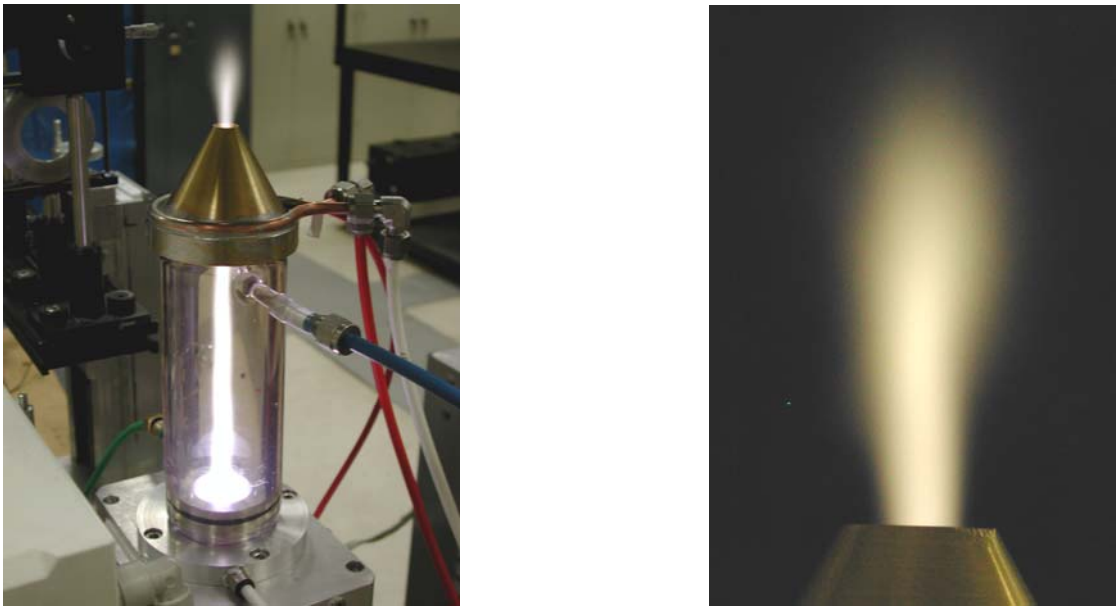

a) ***b)***

Figure 5. a) Microwave plasma torch head, test-section, and accelerating nozzle (exit diameter 1 cm). b) air plasma plume at the exit of the 1 cm diameter nozzle.

Unfortunately, we encountered problems with the 5 kW magnetrons: several of them have consecutively broken due to the reflected microwaves. The fragile 5 kW magnetron was therefore replaced with the sturdy 1 kW magnetron typically used in the microwave ovens which is more resistant to the reflected waves. On the other hand, it provides substantially lower power into the plasma, for it is not well matched for our torch system and the efficiency of the magnetron is relatively low (<50%).

We performed the calibration of the output microwave power and the reflected power as a function of the magnetron input power. The output power is more than 2x lower than the magnetron input power (due to the low efficiency of the magnetron). The real power going to plasma is further lowered by the reflected power due to the imperfect matching:

$$P_{plas} = P_{out} - P_{refl.} \qquad (1)$$

These powers corresponding to two tested experiments conditions are summarized in Table 1.

Table 1. Magnetron input and output powers, and the real power going into the plasma for both experimental conditions.

Experiment	Input P [W]	Output P [W]	Reflected P [W]	Plasma P [W]
1	922	400	38	362
2	1045	469	7	462

So the plasma powers of 362 and 462 W of course cannot preheat the gas to the previously obtained high temperatures (2000 K obtained with 1.4 kW of MW plasma power, after the cooling test section); nevertheless we tested the typical properties of the air preheated in this way.

3.3.1. Corona as a temperature probe in the preheated air

The microwave plasma temperature can be determined by OES method by comparing the measured and simulated emission spectra. This method is very convenient but sometimes overestimates the temperature if determined from the emission spectra of radicals (e.g. CN, NO, OH). The radicals can gain energy in the chemical process of their production, which can contribute to the elevated temperature. This phenomenon was observed by other authors [4], as well as our previous investigations [5]. Therefore we determine the temperature of the plasma generated in air from N_2 spectrum only, since N_2 molecules are present in the feeding gas and are not produced by chemical processes in the plasma. In near-LTE MW plasma generated in air, however, the excitation of N_2 takes place at the temperatures above 6000 K [6]. Such high temperatures are hardly reached in our plasma, especially not at low power (362 W). As a consequence, there is no emission of N_2 in air. At higher powers we just observe the emission of NO and OH radicals and weak noisy O_2, so there is no appropriate radiation for a reliable OES diagnostics. The emission spectra of the low power (362 W, 8 slpm) MW air plasma shown in Figure 6 demonstrate but the continuum radiation.

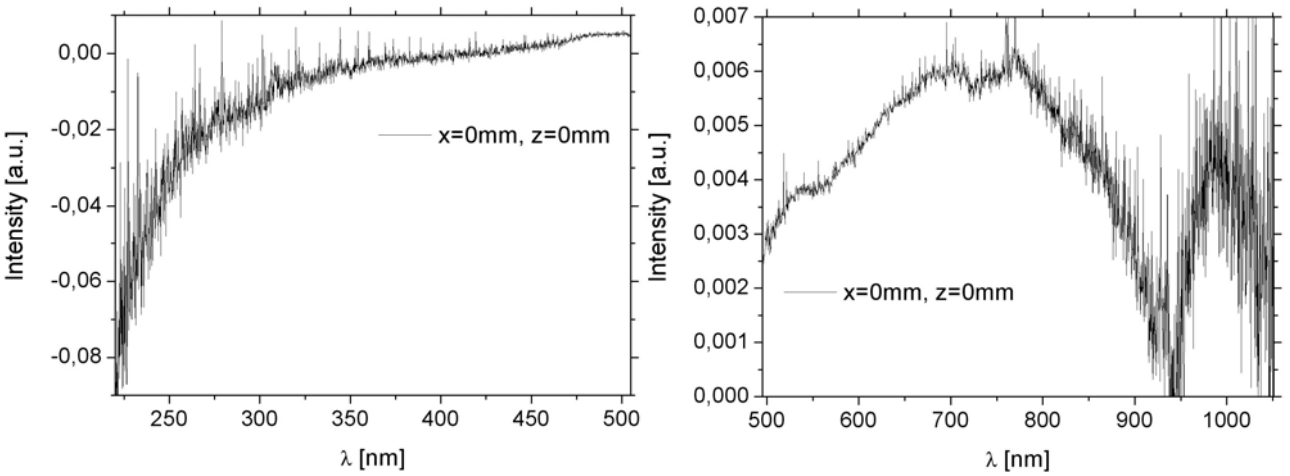

Figure 6. UV and VIS emission spectra of the MW air plasma (362 W, 8 slpm).

On the other hand, it is known that N_2^* is produced in non-equilibrium air plasmas, e.g. in the corona discharge. In this strongly nonequilibrium discharge, the gas temperature is low (almost room temperature) but the high temperature of electrons is sufficient for the excitation of N_2. In the discharges at atmospheric pressure, the rotational temperature balances with the temperature of the surrounding gas. So if we put a needle electrode with DC corona discharge directly into the MW plasma (Figure 7), N_2^* is produced by electron excitation but its rotational temperature is balanced with the surrounding gas temperature – in our case, the temperature of the MW air plasma. The cold

corona discharge does not significantly contribute to the increase of the gas temperature. So, by combining the MW plasma with corona, we can determine the temperature of MW plasma (as a rotational temperature of N_2^*). A journal publication of this novel diagnostics method is being prepared.

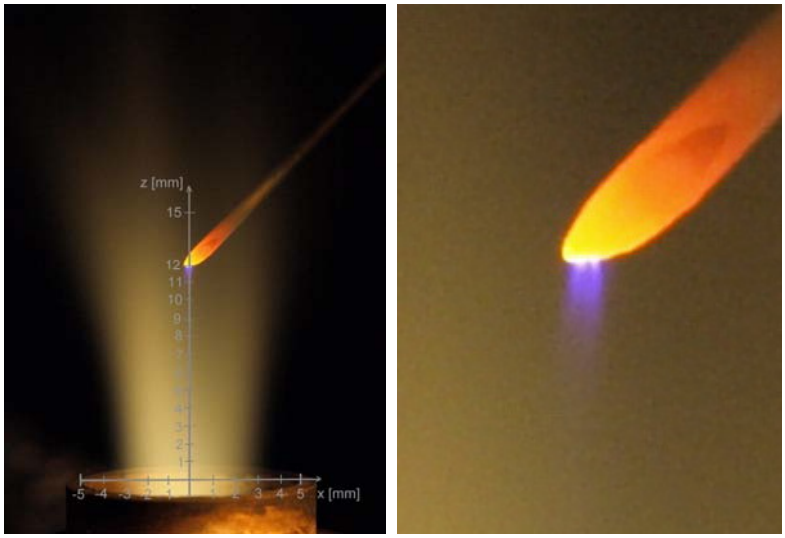

Figure 7. Positive DC corona discharge in the MW air plasma, with indicated dimensions (left) and a detail (right).

The typical OES spectra of positive DC corona discharge (5 kV) in the MW preheated air (362 W, 8 slpm) is shown in Figure 8. A very distinct N_2 ($C^3\Pi_u$-$B^3\Pi_g$) system applicable for temperature measurements was detected in the UV, with the strongest intensity at 337 nm (0-0 vibrational band).

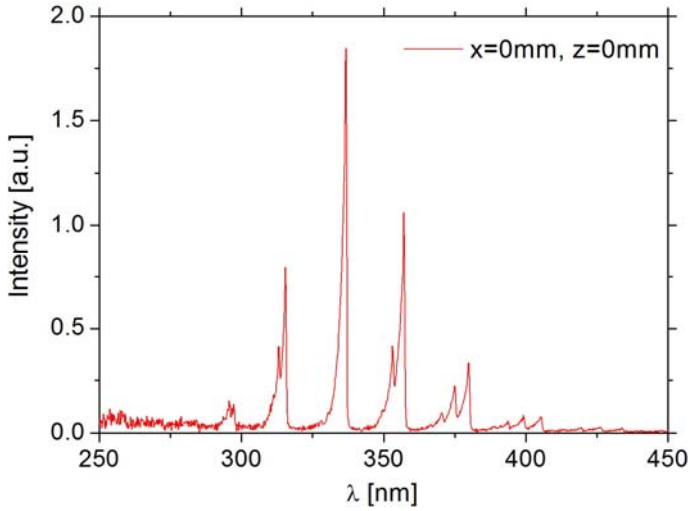

Figure 8. Typical UV emission spectra of the positive DC corona (5 kV) in the MW air plasma (362 W, 8 slpm).

4. Results and Discussion

4.1. DC discharge types and their transitions

When a high voltage of a few kV is applied to the point electrode, a corona discharge appears on the point, further developing to *streamer corona (SC)*. SC is typical with small current pulses of streamers (~10 mA) with a repetitive frequency of 10-30 kHz, during which the discharge voltage remains fairly constant [7]. As the voltage is further increased (to ~8 kV in 6 mm gap), the streamers establish a conductive channel that leads to a spark formation. During the streamer-to-spark transition the local gas heating in the streamer-induced channel decreases the gas density N, thus enhancing the reduced electric field E/N. Since E/N is the main parameter controlling the rate of electron-impact reactions, especially ionization, this state leads to an enhanced ionization, resulting in a spark breakdown with excessive current pulse [8]. Other mechanisms related to the accumulation of active particles changing the balance between the rates of generation and loss of electrons due to an enhancement of the detachment, stepwise and associative ionization, etc. can take place as well [9].

In our case, the spark pulse current is limited by 1) the ballast resistor R that drops the voltage as the current increases, and 2) the capacity C between the electrodes that is small (order of 10 pF). Thus, even if the sparks forms, it is only transient since the discharged energy is small (~0.1-1 mJ). C is a sum of the internal capacity of the discharge gap (C_{int} ~1 pF) and the capacities of the high voltage cable (C_{cable} ≈20 pF) and the probe (C_{probe} = 3 pF), as shown in Figure 3. After the pulse, C is recharged by a growing potential on the stressed electrode. As soon as C is charged enough again, it triggers a new pulse. This *transient spark* (TS) becomes then a repetitive streamer-to-spark transition discharge, with each spark pulse (~1 A) preceded by one or a sequence of streamer pulses [7]. The repetitive frequency of pulses is 0.5-10 kHz, and increases with the growing applied voltage. Thanks to the very short pulse duration (~10-100 ns) given by the small C and a limiting R, the plasma cannot reach LTE conditions.

By setting the values of R and C (C can be set by the length of the HV cable or by filtering $C_{cable} + C_{probe}$ by a small resistor r put very near the high voltage electrode) we can either obtain the TS pulses and control their amplitude and frequency, or obtain a continuous discharge. This pulse-less discharge typically appears after the spark pulse if $R \leq 2$ MΩ and $f > 5$ kHz, and so the voltage drops to a certain small value but not zero, high enough though to sustain a small current (~mA). It has a character of a *glow discharge* (GD), and is typical with constant voltage and current (~1-10 mA), a cathode fall of several hundreds V, and a luminous positive column that occupies most of the gap space. Its current-voltage characteristic is descending. GD is in detail described in the next section and in [10-12]. Its current is determined by the applied voltage and the value of R that prevents its transition back to TS but allows small current. When its current is progressively risen up to ~100-1000 mA, GD smoothly transits towards a continuous arc.

4.2. DC glow discharge in ambient air

Single DC and pulsed glow discharges in air and nitrogen at atmospheric pressure have been extensively studied at Stanford University within the framework of the AFOSR projects, both experimentally and theoretically. [1-2, 10-14] The objective of these studies was to provide a clear

understanding of the mechanisms of ionization and recombination in atmospheric pressure air plasmas. In our investigations of the DC glow discharges following these former studies we focused at DC glow discharges at low currents and in ambient air.

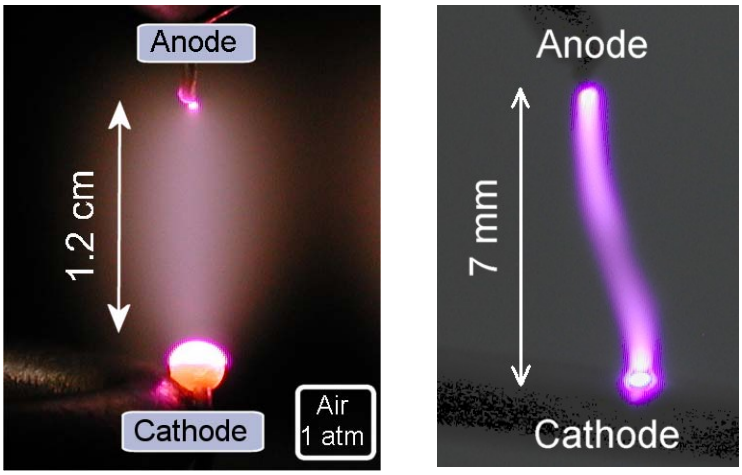

a) Pt-Pt pin electrodes, I=100 mA, U = 1.5 kV, d=1.2 cm

b) Stainless needle – Cu plate, I=5 mA, U = 1.7 kV, d=0.7 cm

Figure 9. DC glow discharge in air at room temperature and atmospheric pressure.

4.2.1. Electrical characteristics

The DC atmospheric pressure air discharge under study is a stable continuous discharge regime with no pulses. It operates with DC currents from 1.6 to several hundreds of mA, and DC voltages from a few kilovolts to a few hundred volts. The gap length (interelectrode distance) can be varied from 1 mm to a few cm, depending on the gas flow conditions and the current. Figure 9 shows photographs of DC glow discharges in ambient air at atmospheric pressure operating at low flow velocity (< 0.2 m/s) and currents of 100 mA and 5 mA.

The discharge is ignited by a streamer-to-spark transition, as explained in section 4.1 but the ballast resistor immediately limits the spark current. However, the ballast resistor is chosen experimentally so that the limiting current is large enough that the discharge, after extinction of the initial spark phase, enters a state of permanent conduction. The ballast-limited current then controls this pulse-less discharge regime.

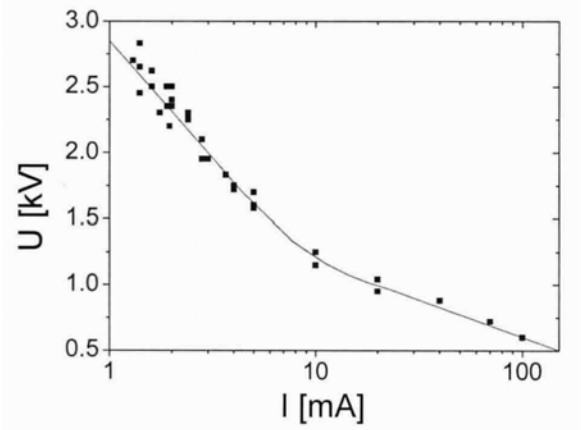

Figure 10. Voltage-current characteristic of the DC discharge in ambient air. Gap distance d = 7 mm.

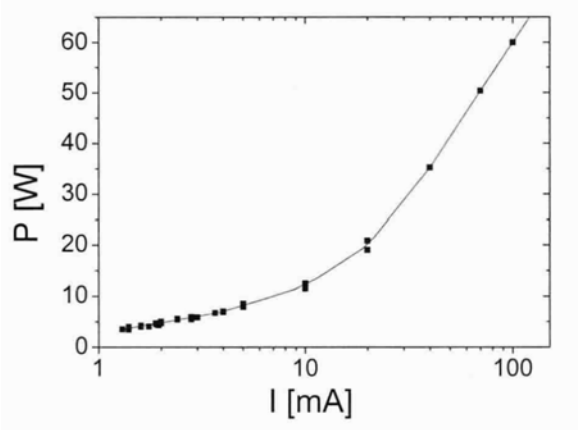

Figure 11. Discharge power as a function of current. Gap distance d = 7 mm.

The voltage-current characteristic of the discharge in ambient air is descending, as shown in Figure 10. In contrast, the discharge power increases with the current, as shown in Figure 11, reaching values of 3-60 W.

4.2.2. Emission spectra and vibrational and rotational temperatures

We recorded the spectra emitted by the DC air GD in the 200-1050 nm region for various discharge parameters, as shown in Figure 12 together with the emission spectra of transient spark. The N_2 ($C^3\Pi_u$-$B^3\Pi_g$) and optionally NO γ ($A^2\Sigma^+$-$X^2\Pi_r$) spectral systems were then used to measure the rotational and vibrational temperatures, T_r and T_v, by comparison with simulated spectra, as indicated in Figure 13. The gas temperature T_g, measured at the centerline of the discharge column, varies typically in the range of 1500-2500 K. The current and the gas flow velocity control the power density deposited in the discharge, and thus the gas heating. At a given low flow velocity of ambient air through the discharge, T_g increases and T_v decreases with increasing current (Figure 14). The measured T_v of the excited states are around 4000 K. These temperatures are higher than the gas temperature and therefore suggest that the plasma is in a state of thermal nonequilibrium. This thermal nonequilibrium indicates that the discharge is a glow and not an arc.

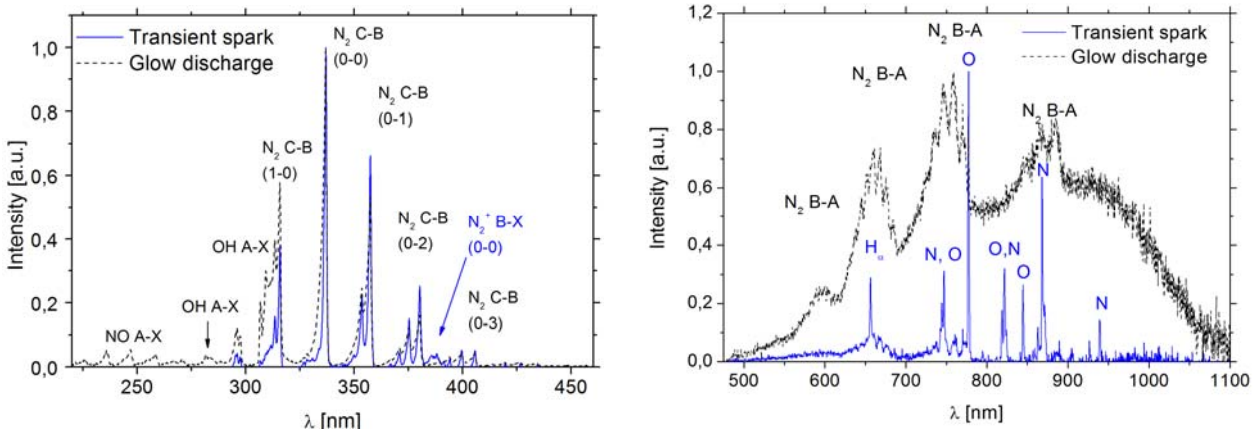

Figure 12. Typical emission spectra of DC discharges in UV and VIS-NIR region. Gap: 4 mm; TS: 1 kHz, I_{max}=1.5 A; GD: I=6 mA.

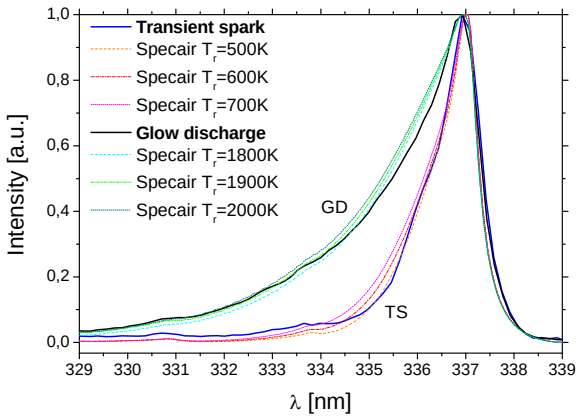

Figure 13. Determination of rotational temperatures from N2 2nd positive system, 0-0 vibrational band. Gap: 4 mm; TS: 1 kHz, Imax=1.5 A; GD: I=6 mA.

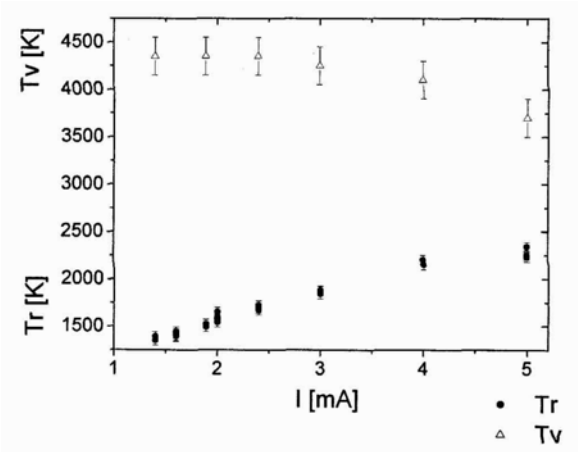

Figure 14. Rotational and vibrational temperatures as functions of the discharge current in ambient steady-state air, interelectrode distance d = 7 mm.

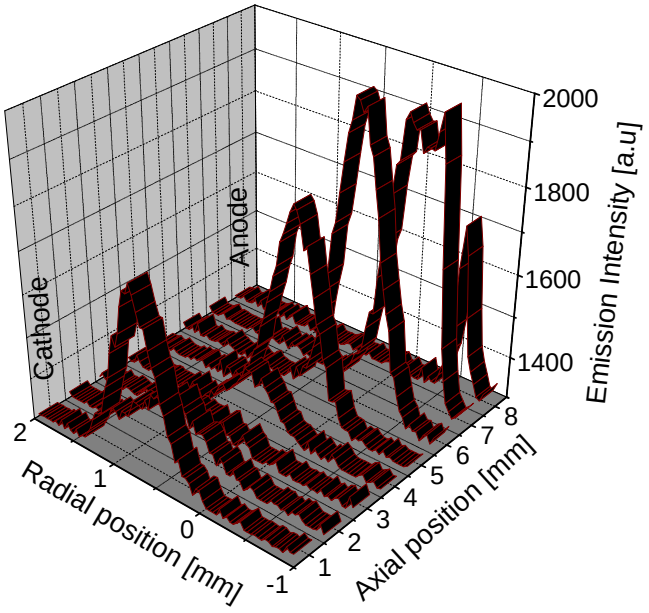

Figure 15. 2D radial-axial emission intensity profile at λ=337 nm. DC glow discharge in ambient air, I=5 mA, gap 7 mm. Radial profiles at each axial position represent integrated intensity over 1 mm thick axial plasma slab.

Besides temperature measurements, optical emission spectroscopy diagnostics also provides the spatial distributions of emission intensity. The axial emission intensity profiles indicate the stratification into dark and bright layers, typical of low pressure glow discharges [15]. The 2-dimensional radial-axial emission intensity distributions of GD with the discharge current I = 5 mA and gap length 7 mm were recorded at 337 nm (N_2 C-B (0-0) band), as shown in Figure 15. An intensity peak at the cathode vicinity, as well as the intensity minimum around 2.5-3 mm from the cathode, were distinguished. They can be also observed visually as brighter and darker spaces. The bright and dark regions near the cathode are reminiscent of the negative glow and the Faraday dark space. Nevertheless, the positive column occupies most of the interelectrode space. The cathode layers are concentrated in the immediate vicinity of the cathode, thus suggesting that the positive column occupies most of the interelectrode space.

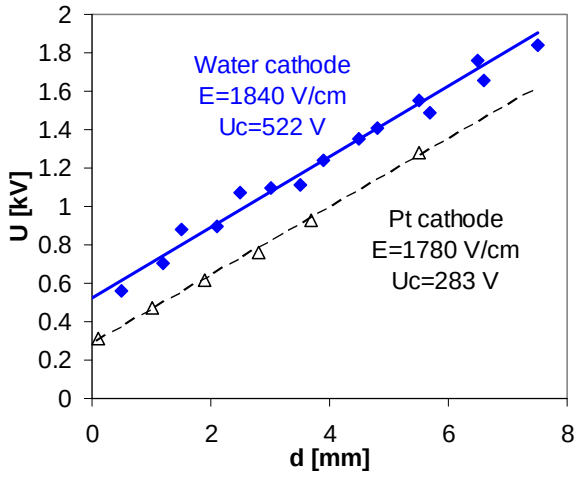

Figure 16. Discharge voltage as a function of the gap distance of GD (5 mA) in needle – water vs. needle – Pt cathode gaps. Corresponding electric fields E and cathode falls U_C are indicated.

This observation was confirmed by electrical measurements. Measurements of the floating plasma potential along the discharge axis by means of a platinum pin probe enable us to calculate the electric field strength E with better than 10% uncertainty. The measured electric field is approximately uniform in the positive column (Figure 16), except within the ~1 mm region close to the cathode. It decreases from 3000 to 300 V/cm as the discharge current is increased, thus leading to a falling voltage-current characteristic (Figure 10). The voltage drop across the cathode region is about 280 V or 380 V, values typical of the cathode fall in air glow discharges with Pt or Cu electrodes at low pressures [15]. With water cathode, the cathode fall is substantially larger: 522 V.

4.2.3. Electronic temperature and radical concentration measurement

Spectra with several emission systems enable estimating T_{el}, the electronic excitation temperature, which corresponds to the Boltzmann distribution among excited electronic states. This T_{el} may be close to T_e, the temperature of free electrons. Nonequilibrium plasmas typically have $T_e > T_{el} > T_v > T_r$. [5-6] We estimated T_{el} in GD that demonstrated N_2 2nd positive, NO γ, and OH system in the UV spectra. By changing T_{el} in the modeled spectrum, relative intensities of N_2 2nd positive and NO γ systems varied and we found the best fit of the experimental spectrum at T_{el} = 9800 K (after having T_r and T_v already determined), as shown in Figure 17. We may presume T_e higher than T_{el}.

Nonetheless, the reliability of this described method is limited, because it is based on N_2 2nd positive and NO γ systems that may not be in chemical equilibrium. NO are radicals formed by chemical pathways, and thus may posses certain chemical energy. They also may not follow the Boltzmann distribution of electronic excited states.

After having $T_g = T_r$, T_v, and presumed T_{el} of GD, and assuming the Boltzmann distribution of all excited electronic states, we can estimate the concentration of OH radicals from the intensity of the OH A-X band. Since OH A-X band partly overlaps with the N_2 2nd positive 1-0 and 2-1 bands, this method is very sensitive to T_{el} and T_v. SPECAIR uses the database of an initial LTE species distribution at various temperatures (not specific to the excitation). In all air modeled spectra we used this database for air with 42% relative humidity. However, even after T_{el} being found, the OH modeled spectrum could not reach the value of the measured intensity of OH bands, since the real concentration of water vapors in the discharge was higher (T_g=1900 K caused a strong water evaporation and dissociation). So we increased the initial OH concentration in this database until a good match with the measured OH bands was reached, as shown in Figure 18. The corresponding OH concentration was found: [OH]≈0.8 % vol. that corresponds to approximately 3×10^{16} cm^{-3} (at 1900 K, neutral density $N=3.86\times10^{18}$ cm^{-3}). Keeping in mind the limitations of the determining T_{el} and the Boltzmann distribution assumptions, this calculated OH concentration should be taken as a very rough estimate, just indicating the order of magnitude. However, such concentration is very high and so explains the dominant role of OH radicals in bio-decontamination or flue gas cleaning applications.

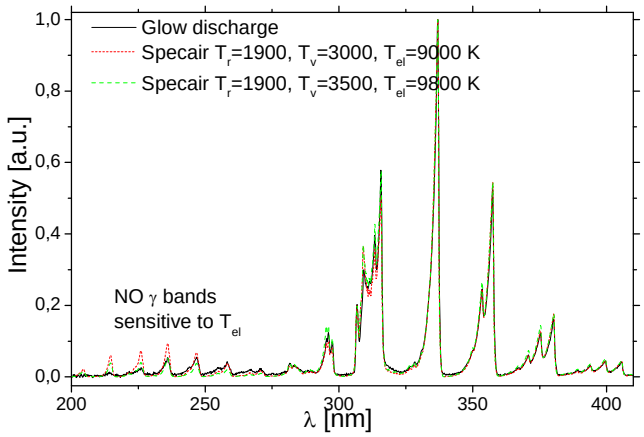

Figure 17. Estimation of T_{el} from the complex glow discharge spectra. Gap: 4 mm; I=6 mA.

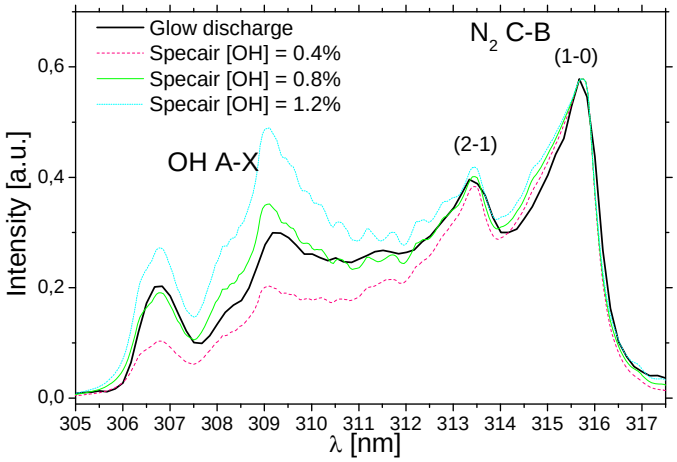

Figure 18. Fitting OH bands to estimate the OH concentration in the glow discharge. Gap: 4 mm; I=6 mA.

4.2.4. Measurement of the plasma size and electron density

The radial emission intensity profiles of N_2 ($C^3\Pi_u$-$B^3\Pi_g$), NO γ ($A^2\Sigma^+$-$X^2\Pi_r$) and OH ($A^2\Sigma^+$-$X^2\Pi_{3/2}$) systems were used to measure the diameter of the positive column. The diameter of the discharge in air measured by total emission with a 337 nm filter (corresponds to N_2 $C^3\Pi_u$-$B^3\Pi_g$ (0,0) transition) is approximately 1.7 mm for the current of 100 mA, while only 0.53 mm for *I*=5 mA. In Figure 9a, the discharge in air at 100 mA appears to be wider. This effect is due to the presence of a halo around the discharge produced by NO_2 emission in the surrounding air environment heated by the discharge.

The diameter of the positive column of the discharge can be defined as the full width of half maximum (FWHM) of the radial electron density profile. Although the direct measurement of the electron density in atmospheric pressure plasmas is difficult, the Abel-inverted radial emission intensity profiles of various excited species in the discharge column (most typically N_2 $C^3\Pi_u$-$B^3\Pi_g$)

can be used to measure the discharge diameter *D*. Abel inversion was applied because the discharge has a radial symmetry.

This approach assumes that the emission profiles are representative of the electron density profile. We confirmed this assumption experimentally in an atmospheric pressure nitrogen DC discharge where we have obtained reasonable agreement between various emission profiles of excited N_2 and N_2^+ states, and the electron density profile calculated from the N_2^+ X (v=0) ion concentration measured by cavity ring-down spectroscopy [16].

Here, in the air discharge, the diameters measured from NO γ and OH are typically about 1.2-1.5 times larger than the diameter measured from N_2. This result can be explained by assuming direct electron impact as the dominant excitation mechanism, and a radially decreasing distribution of electron energies. Electrons with higher energy are needed to excite N_2 $C^3\Pi_u$ state (11 eV), while energies of only about 5.5 and 4 eV are sufficient to excite NO $A^2\Sigma^+A$ and OH $A^2\Sigma^+$ from their ground states. Thus, the spatial extent of the N_2 C-B radiation is narrower than those of NO γ A-X and OH A-X. Nevertheless, the width of the emission profiles of N_2, NO, and OH are within 20-50% of each other and this gives a reasonably accurate estimate of the discharge diameter and related parameters, namely the current density.

The discharge diameter measured as the FWHM of the radial emission profiles than allows estimating the plasma volume. It can also be used to estimate the current density *j* by using a simplified relation

$$j = \frac{I}{\frac{1}{4}\pi D^2}. \qquad (2)$$

The typical GD in ambient air (I = 5 mA) has a diameter D = 0.53 mm, as measured by emission of the N_2 C-B (0,0) band, with the corresponding j = 2.3 A/cm^2. The measured discharge diameters range from 0.4 to 3.3 mm, depending on the current, the gas flow velocity, and the gas temperature. The corresponding current densities j are between 0.1 and 10 A/cm^2 Electron number density n_e is a very important parameter characterizing the plasma and can be derived from the measured current density and electric field strength. The simplest estimate of n_e can be then obtained using the expression for the current density

$$j = n_e e v_d, \qquad (3)$$

where e is the elementary charge and v_d is the electron drift velocity. The electron drift velocity is given by the electron mobility μ_e and the electric field strength E:

$$v_d = \mu_e E. \qquad (4)$$

E was approximately measured from the applied voltage and the column length. μ_e, or rather the product of the μ_e and the pressure p, can be considered constant in our experimental conditions (positive column of an air glow discharge): $\mu_e p = 4.6\times10^5$ cm^{2}TorrV^{-1}s^{-1}. [15] The pressure should be better represented by the gas density N to accommodate for the elevated temperature at p = 1 atm, similar to representing the reduced field as E/N rather than E/p. In N-representation, $\mu_e N = 1.484\times10^{22}$ cm^{-1}V^{-1}s^{-1} in air glow discharges. This value can be then used in the expression of the electron drift velocity and the electron density can be calculated subsequently:

$$n_e = \frac{j}{e\mu_e N \frac{E}{N}}. \qquad (5)$$

Resulting n_e of GD was in the order of 10^{12} -10^{13} cm^{-3}. This value agrees well with the n_e measured by Cavity Ring-Down Spectroscopy of N_2^+, the dominant ion in nitrogen glow discharges. [16] The measured j is lower than the typical current density of arcs. Moreover, the measured cathode fall is typical of glow discharges. The stable operation of this discharge is supposedly provided by the secondary electron emission from the cathode. The high values of n_e at gas temperatures between 1500 and 2500 K confirm the departure from thermal nonequilibrium. (LTE values of n_e in atmospheric pressure air are about 10^2, 10^6, and 10^9 cm^{-3} for temperatures of 1500, 2000, and 2500 K, respectively).

The gap length of GD can be varied up to 10 cm, depending on the flow velocity of the gas and the discharge current. Plasma volumes of ~0.5 cm^3 can be produced in this manner.

4.3. DC Discharges in Fast Flow of Preheated Air

4.3.1. Air preheated to 2000 K

DC discharge experiments were originally also conducted with fast flowing preheated air at ~2000 K. The main reason for going to fast gas flows (20-400 m/s) is that discharges at slow flows result in significant gas heating, especially at high currents where electron number densities of 10^{12} cm^{-3} or higher are achieved. The mechanism of gas heating can be explained as follows.

In the DC discharges, a large fraction of the electron energy is lost via excitation of the vibrational modes of air molecules, mainly N_2. These vibrational modes subsequently relax through collisions with the dominant species, i.e. O, N_2, and O_2. This collisional quenching transfers the energy from vibration into the translational modes of molecules, which results in Joule heating of the gas. This process is called vibrational-translational energy transfer (V-T transfer). In slow air flows, the residence time of the gas in the discharge is long enough to enable the V-T transfer. As a result, the gas is heated.

In fast air flows, on the other hand, the vibrational modes of N_2 have shorter time to relax, hence cannot heat the gas as much over the short residence time between the two electrodes. Thus the temperature in the discharge is almost determined by the inlet gas flow. Yet, it is very difficult to maintain stable DC discharges in fast flows of ambient air. This is because electron attachment is fast, whereas ionization is slow since the reduced field strength E/N (where E is the field strength and N is the gas density) is lower due to the lower gas temperature, hence higher N.

For these reasons, we used a fast flow of preheated air at ~2000 K. At this temperature, electron attachment does not play an important role. Moreover, the density is about seven times lower than at room temperature and the reduced field strength E/N is sufficient to maintain the discharge. When the residence time of the flow in the discharge column is shorter than the characteristic time for V-T relaxation (~ 10 μs) the temperature remains close to 2000 K.

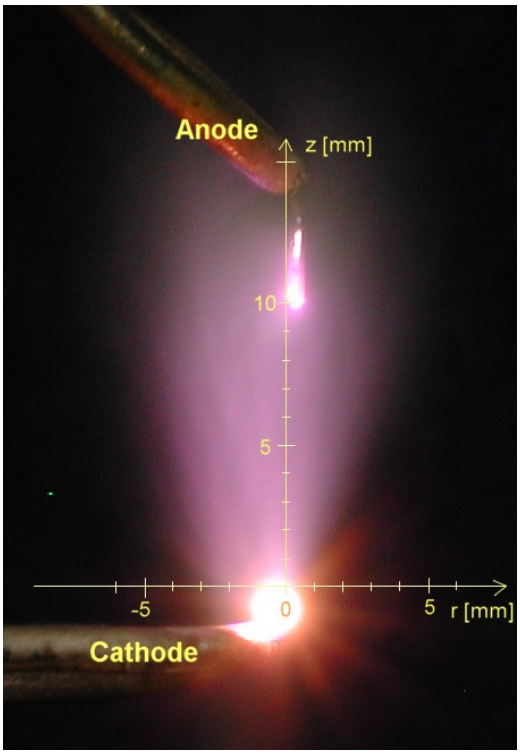

Figure 19. DC glow discharge in air preheated to ~2000 K: I=100 mA, gap 1 cm, vertical upward flow, v=278 m/s.

Figure 19 shows photographs of a microwave air plasma plume preheated to 2000 K with a DC discharge applied. In these experiments, the inter-electrode distance was about 1 cm, and the discharge diameter measured by the emission of the N_2 C-B transition was about 3 mm. The discharge diameter is larger in preheated air than in ambient air. This effect is due to the presence of larger dissipative thermal gradients in the ambient air discharge than in the preheated air plume. So operating in preheated air brings an advantage for volume scaling. On the other hand, it costs more power, especially when accounted for microwave preheating (~1.5 kW).

Preheating to ~2000 K at atmospheric pressure results in ~7x lower *N*, which has practically similar effect as 7x reducing the pressure, in terms of *E/N* and ionization. Reduced pressure would make sense for plasma shielding applications for high altitude aircraft. Such experiments are therefore planned for the next period. However, we must take into account that plasma kinetics at 2000 K and 300 K are not the same, strong electron attachment takes place at room temperature and much more gas heating occurs due to VT transfer.

4.3.1. Air preheated below 2000 K

As described in section 3.3, due to technical problems with 5 kW magnetron we started using 1 kW magnetron, which resulted in substantially lower air preheating. Corona discharge was used as a probe to measure gas temperatures in this case, as explained in section 3.3.1.

The typical OES UV spectrum of positive DC corona discharge (5 kV) in the MW preheated air (362 W, 8 slpm) was shown in Figure 8. A very clear N_2 ($C^3\Pi_u$-$B^3\Pi_g$) system was detected in the UV, with the strongest intensity at 0-0 vibrational band at 337 nm. The gas temperatures of this plasma plume at two powers (362 and 462 W) and the same air flow rate (8 slpm) were determined as rotational temperatures from N_2 ($C^3\Pi_u$-$B^3\Pi_g$) bands. The 1-D and 2-D profiles of the measured gas temperature for both investigated powers are shown in Figure 20. The vertical upward flow velocities were calculated to 7.5 and 9.2 m/s, with respect to the measured temperatures.

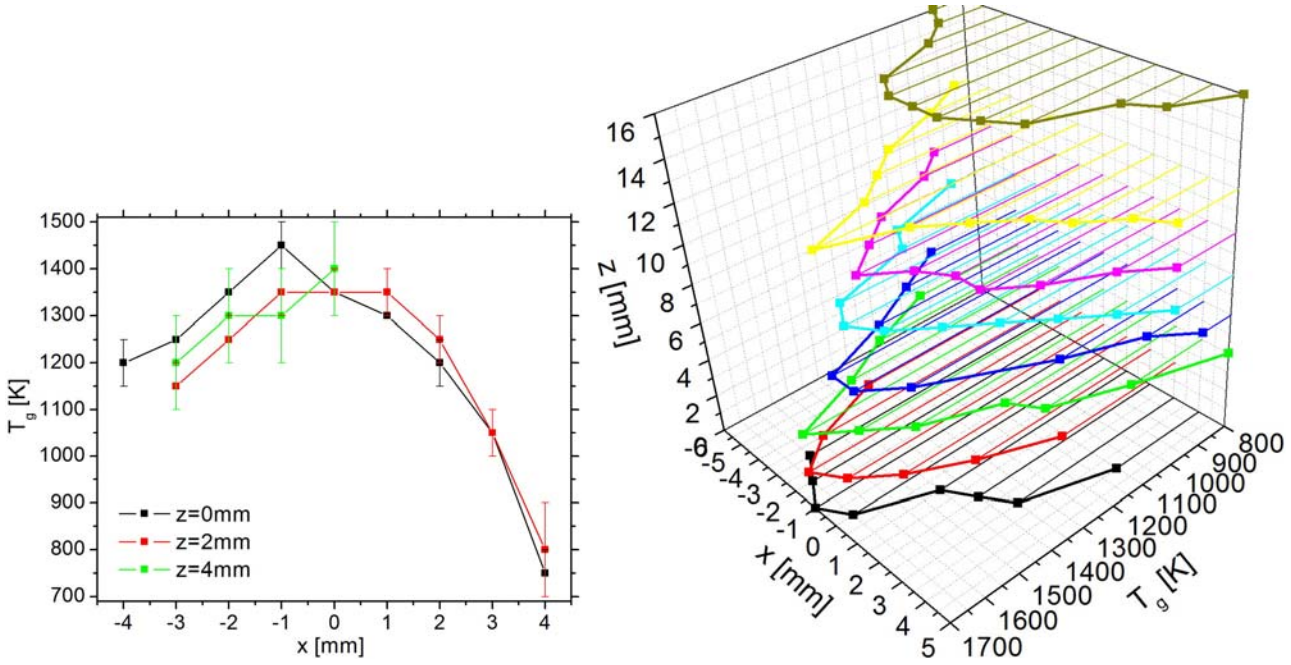

Figure 20. Profiles of T_g in the air plasma plume measured with the corona probe. Left: 1-D radial profile, 362 W, 8 slpm, vertical upward flow, v=7.5 m/s; right: 2-D radial-axial profile, 462 W, 8 slpm, v=9.2 m/s, typical uncertainties 50-100K.

DC glow discharges of two currents (5.5 and 10 mA, corresponding voltages 1.3 and 1.4 kV, respectively) were applied in this preheated air plasma plume (362 W, 8 slpm, 7.5 m/s). The cathode was placed 2 mm above the nozzle exit (z=2 mm) and the needle anode 10 mm above (z=12 mm) at the radial axis of the plasma plume (x=0), as shown in Figure 21. At these low currents, the typical visible violet radiation can only be seen next to the electrodes, unlike in the 100 mA GD in the fast flow (278 m/s) of preheated 2000 K air (Figure 19).

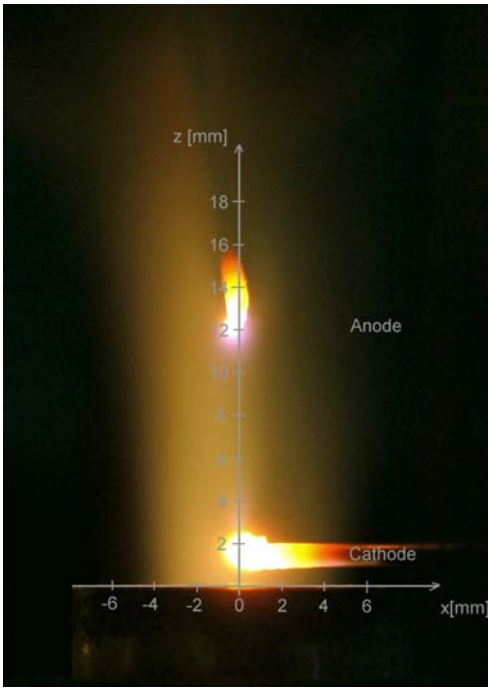

Figure 21. DC glow discharge applied in the air plasma plume (P=362 W, Q=8 slpm, vertical upward flow, v=7.5 m/s); I=5.5 mA, U=1.3 kV.

The example emission spectra of these GDs are shown in Figure 22 in the semi-log scale. Besides N_2, strong NO γ ($A^2\Sigma^+$-$X^2\Pi_r$) radiation can be observed. In addition, we detected OH ($A^2\Sigma^+$-$X^2\Pi_{3/2}$) in the positive column and N_2^+ ($B^2\Sigma_u^+$- $X^2\Sigma_g^+$) at the cathode. N_2 spectra were well used to measure T_g at the cathode and the anode. Unfortunately, N_2 spectra were too weak in the positive column to make reliable temperature measurements; the error bars are as large as 300 K, as shown in Figure 23.

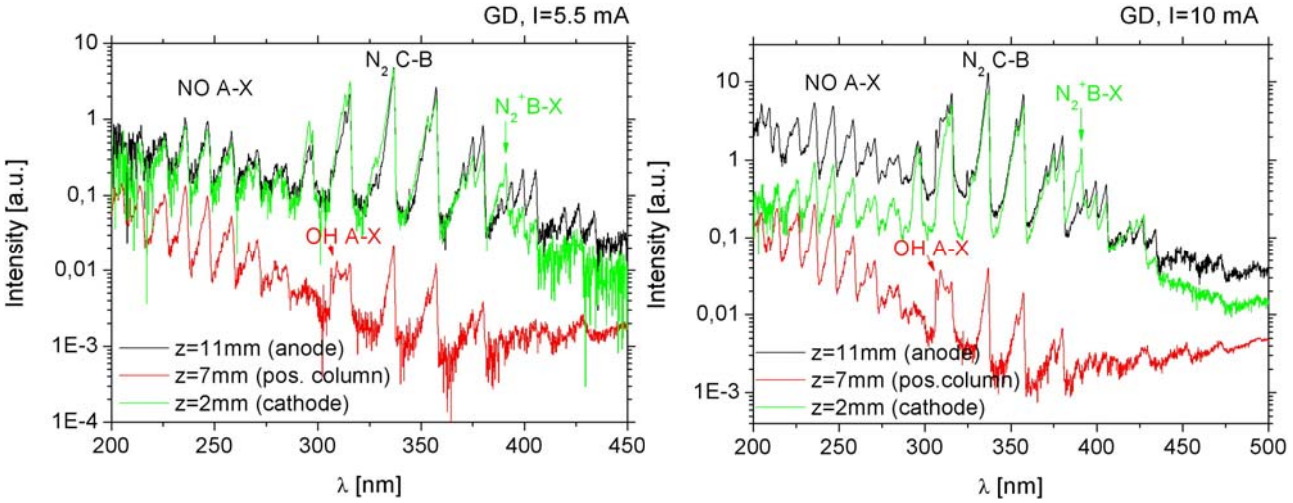

Figure 22. UV emission spectra of the DC glow discharge applied in the air plasma plume (362 W, 8 slpm) shown in semi-log scale; I=5.5 mA, U=1.3 kV (left) and I=10 mA,U=1.4 kV (right).

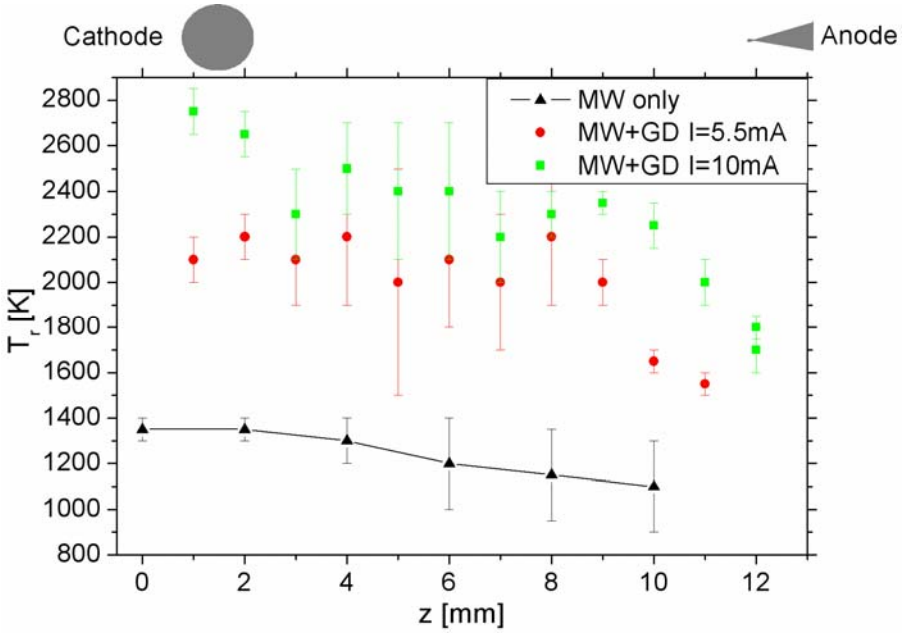

Figure 23. Axial profiles of T_g in the DC glow discharge applied in the MW air plasma plume (362 W, 8 slpm, 7.5 m/s), I=5.5 mA and 10 mA; shown together with the T_g profile of the plume measured by corona probe.

Apparently, the GD gas temperatures are above those of the preheated air plasma. The glow discharge in these flow conditions contributes to the gas heating, since the slow air flow velocity of 7.5 m/s is not sufficient to prevent the VT transfer. Nevertheless, by adjusting the GD current to the flow and temperature of the air plasma we can obtain the desired 2000 K conditions.

4.4. Transient spark

Transient spark (TS) is a filamentary streamer-to-spark transition discharge initiated by a streamer, which transforms to a short spark pulse. Its typical look is shown in the photograph in Figure 24. The typical current and voltage waveforms are shown in Figure 25. The current pulse is due to the discharging of the capacity *C*, composed of the internal capacity of the discharge chamber C_{int}, capacity of the high voltage cable between the ballast resistor *R* and the electrode, and the capacity of the high voltage probe. When *C* is discharged, the current given by

$$I(t) = -C\,\frac{dU}{dt} \tag{6}$$

reaches a high value (~1 A) and the voltage drops to zero due to the resistive fall on the external resistance *R*. Then, during the quenched phase, *C* is recharged by a growing potential *U* on the stressed electrode. The potential *U* grows in time *t* according to the following equation:

$$U(t) = U_0\left[1 - \exp\left(-\frac{t}{RC}\right)\right] \tag{7}$$

where U_o is the high voltage applied to the stressed electrode. Usually, during this relaxation phase when the gap potential reaches a specific threshold, corona discharge appears, and some pre-breakdown streamers. As soon as *C* is sufficiently charged again, it triggers a new pulse. It occurs in time $t=T$, at discharge voltage U_{dis} given according to equation (7) by:

$$U_{dis} = U_0\left[1 - \exp\left(-\frac{T}{RC}\right)\right] \tag{8}$$

From (8) we get the characteristic repetition frequency *f* of this process:

$$f = \frac{1}{T} = \frac{1}{RC\,\ln\left(\frac{U_0}{U_0 - U_{dis}}\right)} \tag{9}$$

For typical *R* and *C*, the repetition frequency *f* is in order of several kHz. However, the measured frequency is not absolutely regular. The TS breakdown voltage U_{dis} may also depend on *f*, especially at higher *f*, when the gap may remain pre-ionized. Thus, the next TS breakdown occurs at lower U_{dis}. Lower U_{dis} consequently increases *f*. As *f* extends a certain value, TS may transform into a pulse-less glow discharge regime with a constant current of few mA. This transition is controlled by the external resistance *R*, the distance between the electrodes, and the gas flow rate. TS discharge regime was first mentioned in [17-18] and further described in [19].

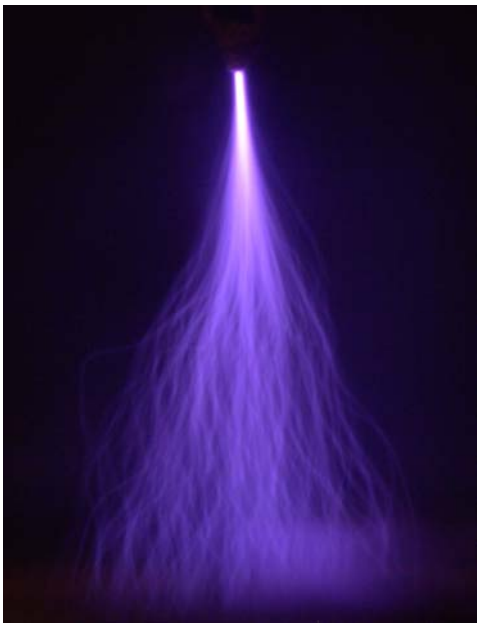

Figure 24. Photograph of TS in positive needle – plane gap of 6 mm, aperture f/4.8. TS: 1.2 kHz, I_{max}=4 A, U=7.5 kV, R=3.5 MΩ, exposure ¼ s, ISO 200.

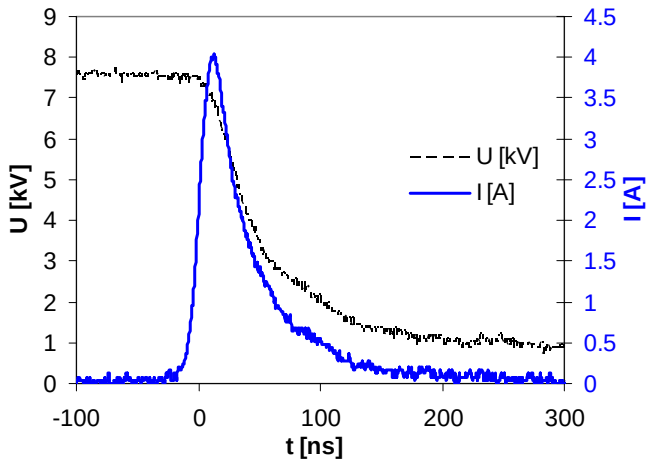

Figure 25. Typical TS current and voltage waveforms, repetition frequency ~5 kHz.

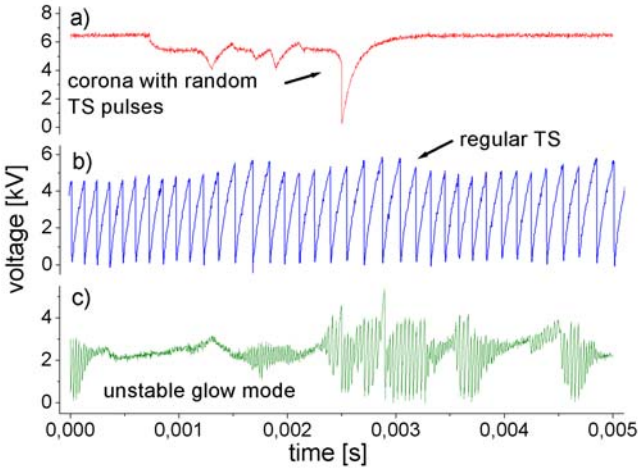

Figure 26. Voltage waveforms of different discharge regimes: a) the first random TS pulses, b) regular TS, c) unstable glow regime.

4.4.1. Transient spark evolution

When the high voltage U_o applied to the stressed electrode is progressively increased, we first observe a streamer corona. When the threshold voltage for TS is reached, a transition to TS occurs at the discharge voltage U_{dis}. The repetition frequency f of these first TS pulses is low and very irregular (Figure 26). Further increase of U_o leads to a monotonous increase of f and TS pulses (Figure 27) become more regular. However, individual pulses are not identical and U_{dis}, as well as f, fluctuate around their average values.

Figure 28 shows the dependence of the average U_{dis} on U_o. The decrease of U_{dis} for higher U_o can be explained by the increasing gas temperature (Figure 32), resulting in a decreasing gas density

N. Since some threshold reduced electric field *E/N* is needed to initiate the TS pulse, *E* and thus also U_{dis} may be now lowered.

With the increase of U_o, the maximum pulse current (I_{max}) decreases (Figure 29) and this decrease is accompanied by the broadening of the pulses (Figure 30). As a result, no significant dependence of the integrated current per pulse *Q* on U_o is observed, and due to the increasing *f* the mean discharge current I_{mean} increases linearly with U_o. When the frequency exceeds ~20 kHz, the discharge tends to convert to the glow regime. However, due to the high value of *R* and the electro-negativity of air, this regime is not stable and the discharge randomly switches between the glow regime and the high frequency TS regime (Figure 26).

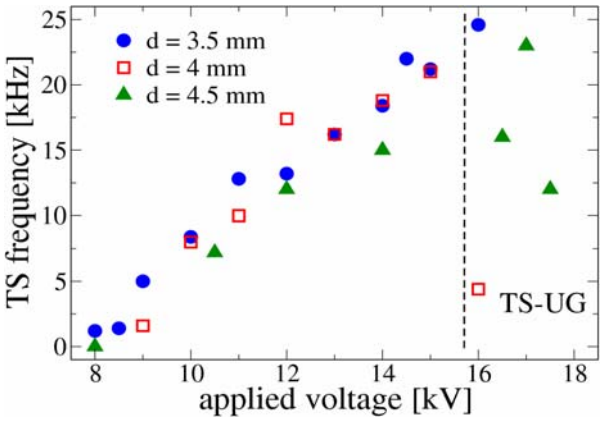

Figure 27. Discharge frequency as a function of the applied voltage U_o, TS-UG represents the region of the unstable glow regime. Experiments with different interelectrode gaps.

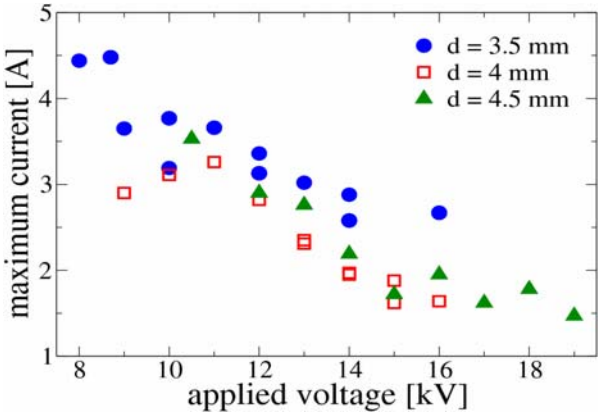

Figure 29. Maximum current in pulse I_{max} as a function of applied voltage U_o.

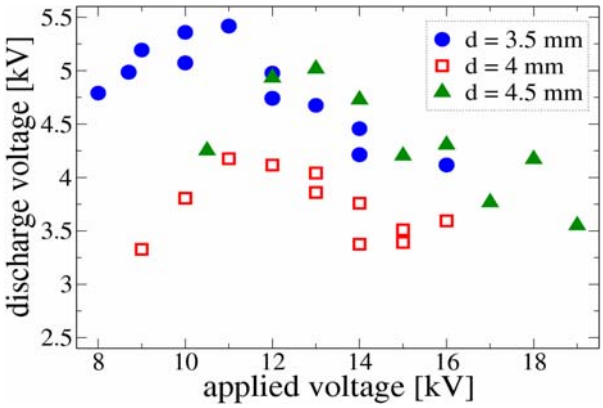

Figure 28. Discharge voltage U_{dis} as a function of applied voltage U_o.

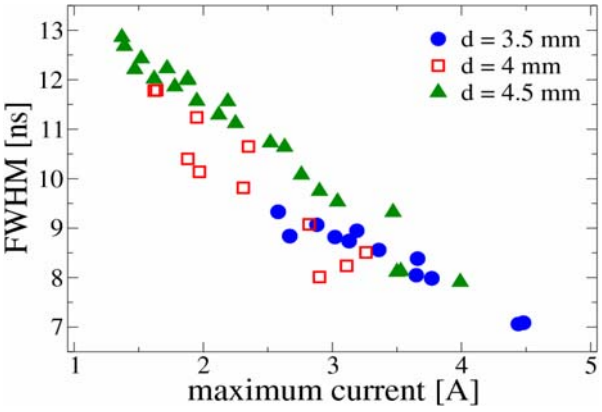

Figure 30. Full width of the pulse at half maximum (FWHM) as a function of the maximum current in the pulse (I_{max}).

TS regime is based on the charging and discharging of *C*. The integrated current *Q* and the energy delivered to the discharge gap per pulse (E_p) are therefore functions of *U* and they can be expressed as

$$Q = CU \qquad (10)$$

and

$$E_p = ½\, CU^2. \qquad (11)$$

The knowledge of the value of *C* is therefore important for the description and characterization of TS. First, we calculated *C* by fitting the obtained current waveforms with current obtained as a negative derivate of the measured voltage waveforms, equation (6). By this way we found *C* to be

6.3±0.3 pF. The values of Q and E_p calculated from equations (10) and (11), respectively, using this value of C are in agreement with Q and E_p obtained by the integration of $I(t)$ and $U(t)I(t)$ for the whole period of the current pulse. On the other hand, this value of C significantly overestimates the TS repetition frequency calculated from equation (9).

We therefore calculated C also from the growth of the voltage on the stressed electrode during the relaxation period, equation (7). We obtained another value of C = 14±1 pF, which enables a correct calculation of f. As a result, we have two values of C, the lower one suitable for the description of discharging event and the second one suitable for the description of charging period.

Further experiments with applying various separating resistors r enabled better understanding of this apparent discrepancy. The role of r is to partially or completely filter the influence of the capacity of the high voltage cable (C_{cable}~20 pF) that substantially contributes to the total discharging capacity C. We tested resistors with various values, from 68 Ω up to 11 MΩ. The results of these tests need subjecting to further analysis and will be described in the next report.

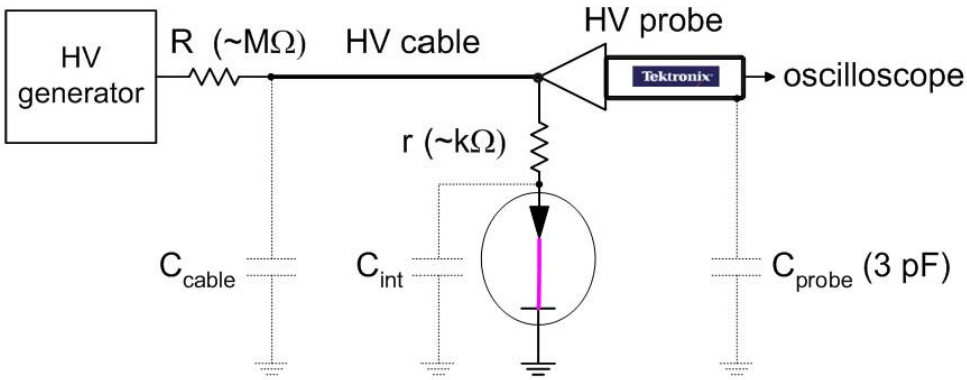

Figure 31. Separating resistor r in the schematic of the electrical circuit of DC discharges.

4.4.2. Emission spectra of TS and temperature measurements

In the UV-VIS emission spectra of TS (shown together with GD in Figure 12), the strongest lines observed can be attributed to the emission of N_2 2nd positive system ($C^3\Pi_u$ - $B^3\Pi_g$) and atomic O line (at 777 nm). Emission of N_2 1st positive system ($B^3\Pi_g$ - $A^3\Sigma^+$), N_2^+ 1st negative system ($B^2\Sigma^+$ - $X^2\Sigma^+$), and atomic N lines is also observed. The presence of N_2^+ and atomic lines indicate that the plasma has high electron temperature and a significant level of non-equilibrium. Non-equilibrium conditions were also confirmed by a difference between the vibrational (T_v) and rotational (T_r) temperatures obtained by fitting the experimental spectra of N_2 2nd positive system with the simulated ones (using the Specair program [3], as shown together with GD in Figure 13**.**

The degree of non-equilibrium decreases with increasing U_o, because T_r increases from about 500 K to 1500 K (Figure 32) and T_v increases from about 3800 K to 5000 K (Figure 33). On the other hand, the mean electron temperature T_e most probably decreases with increasing U_o, since the intensity of atomic O emission per pulse decreases with U_o (Figure 34). The unstable glow regime probably leads to an even more significant decrease of T_e, because in this regime, the emission of N_2 2nd positive system decreases remarkably.

The temporal emission profiles obtained using the PMT measurements also reveal that the maximum intensity of emission lags approximately 60 ns behind the current pulse maximum and the emission of N_2 2nd positive system is quenched faster than the emission of atomic O (Figure 35).

In the glow discharge, a large fraction of the electron energy is lost via excitation of the vibrational modes of air molecules, mainly N_2. These vibrational modes subsequently relax through collisions with the dominant species. The collisional quenching transfers the energy from vibration into the translational modes of molecules, which results in Joule heating of the gas. That is why total power of GD is 5-60 W, depending on the current. The typical time scales of this vibrational-translational (VT) energy transfer in atmospheric air are 10-100 μs.

On the other hand, in the short pulses of TS (pulse duration ~10-100 ns), this VT transfer does not have sufficient time to develop during the discharge pulse. It can only affect the relaxation phase between the pulses. But there, its effect on the gas heating is weak because its time scales are on the contrary much shorter that the typical length of the relaxation period (with the repetitive frequency of some ~1 kHz). Therefore T_g remains fairly low in TS, despite the electrons have high energies. This is a key phenomenon that makes TS discharge very interesting for its low power budget: the discharged energy in one TS pulse is small (~0.1-1 mJ) and the total power, depending on pulse frequency, is 0.1-2 W.

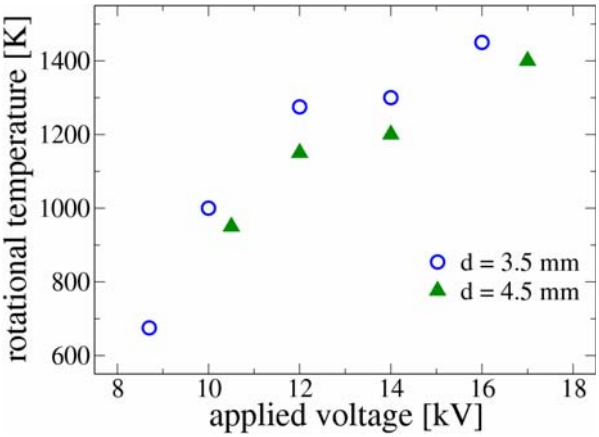

Figure 32. Rotational temperature measured from N_2 (C-B, 0-0) as a function of U_o.

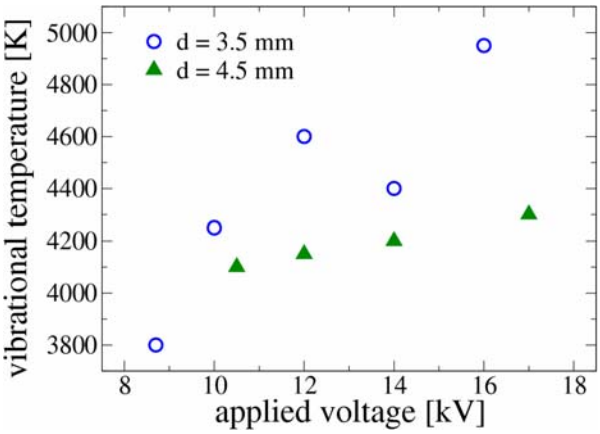

Figure 33. Vibrational temperature of N_2(C) species as a function of U_o.

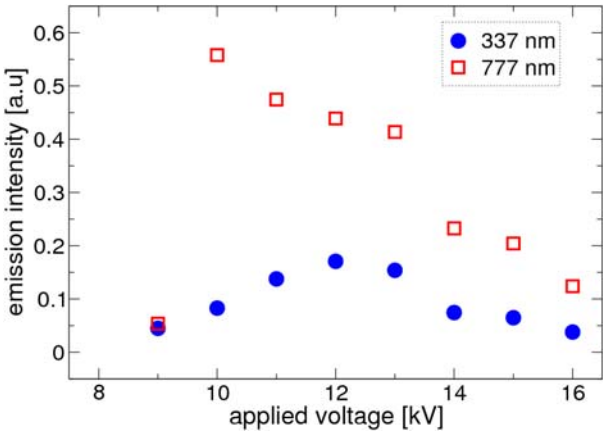

Figure 34. Maximum of emission of N_2 (C-B, 0-0) (337 nm) and O* (777 nm) obtained by PMT as a function of U_o, d = 4 mm.

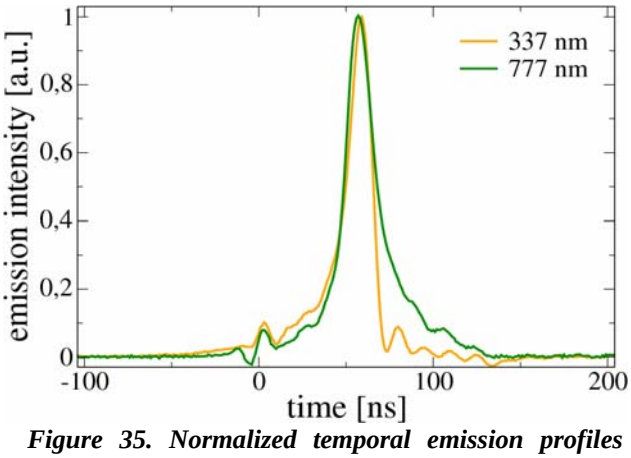

Figure 35. Normalized temporal emission profiles obtained by PMT with filter for N_2 (C-B, 0-0) (337 nm) and O* (777 nm), time t = 0 ns represents the maximum of the current pulse.

4.4.3. ICCD camera preliminary measurements

Recently we obtained an intensified CCD camera enabling gating as short as 2 ns. This was mounted on a 2-m monochromator to obtain high spectral and temporal resolution of the very short processes occurring during the TS pulse evolution. After mounting the appropriate optical components and calibrating the new optical system for wavelength and intensity, we obtained the first preliminary results of the temporal evolution of species during the TS pulse. The total emission intensity of the TS pulse obtained at 0-order of the monochromator is shown in Figure 36 together with voltage and current pulses. Similar temporal evolutions for H, N_2 1^{st} positive system, N and O are shown in Figure 37. The total emission and most of the specific excited species decay exponentially in time. Excited O radicals have a maximum intensity at about 50 ns after the pulse and then exponentially decay.

These preliminary results are very interesting but have one principal drawback – they only show the evolution of processes and radiative species starting ~20 ns after the origin of the current pulse, as can be observed from Figure 36. This is due to problematic triggering of the camera. At present, we trigger by the current pulse itself. Yet, the current pulse travels into the camera through the coaxial cable that causes the first delay of about 10 ns (typical delay of coaxial cables is ~5 ns/m). Then there is a characteristic insertion delay of the camera of ~35-40 ns, making together 45-50 ns. On the other hand this large delay is partially compensated by leading the light through ~8 m long path, delaying it by ~25 ns. However, we still obtain a ~20-25 ns blind period at the beginning of the TS pulse that the camera does not detect. It seems that N_2 second positive system is dominantly radiated just in this blind period, so almost none could be seen after 20 ns. We have tried triggering the camera with the preceding TS pulse but this is extremely difficult because the frequency of pulses is not absolutely regular and the probability of correct delaying and synchronizing a 2-ns window to the beginning of the next pulse is very low.

The preliminary results indicate that ultra fast resolved temporal evolution of emission spectra and radiation from TS has an enormous potential for deeper understanding the elementary processes occurring in this discharge. Of course, this objective requires a lot of further work and coping with many challenges. Unfortunately, the ICCD camera was then twice broken and repaired, which postponed the planned experiments.

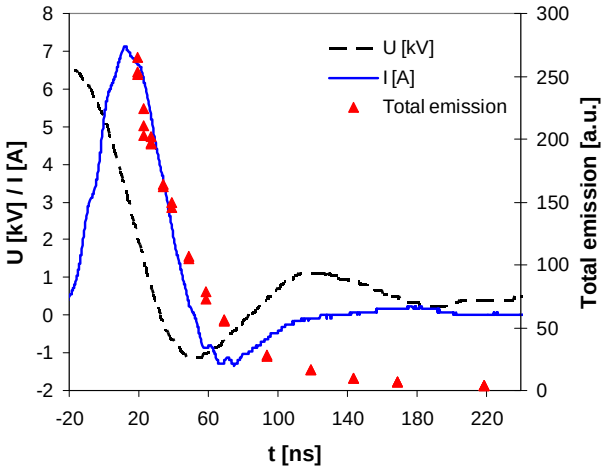

Figure 36. Temporal evolution of the total emission intenisty of the TS measured by ICCD shown together with the voltage and current waveforms.

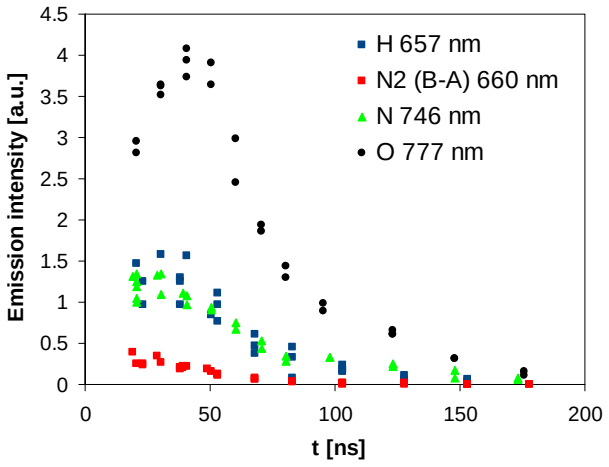

Figure 37. Temporal evolution of the emission intenisty of the TS measured by ICCD at specific wavelengths.

4.4.4. Electron density in TS

In order to calculate the electron density n_e in TS, we used a similar approach as with the glow discharge (section 4.2.4). The concentration of electrons can be obtained from the equation:

$$n_e(t) = \frac{I(t)}{S e v_d(t)} \tag{12}$$

where $I(t)$ represents the discharge current in time, e is an elementary charge, S is a cross-sectional area of the discharge channel, and $v_d(t)$ represents a drift velocity of electrons in time. This approach assumes that plasma can be approximated by a column with a constant diameter. Such a model is a good approximation if E/N is constant along the length of this column. In any case, calculated n_e represents an average density in this column. Such an approximation is sufficient for GD. The situation in TS is much more complicated. First, the current changes in time. Second, due to time variations of E/N, $v_d(t)$ also changes in time. Finally, the spatial distribution of E/N and electrons is also more complicated if compared to GD. This problem will be discussed later.

On the first look it seems there should be no problem to obtain $I(t)$ from our measurements. However, there is difference of several orders of magnitudes between the current during the spark pulse (~A) and shortly before the corona to TS transition (~μA). So we cannot measure both these currents accurately enough. Moreover, equation (6) describes the current only during the discharging of the internal capacity of the chamber after development of the conductive plasma channel. Thus, we first should find a better approximation of $I(t)$ in TS.

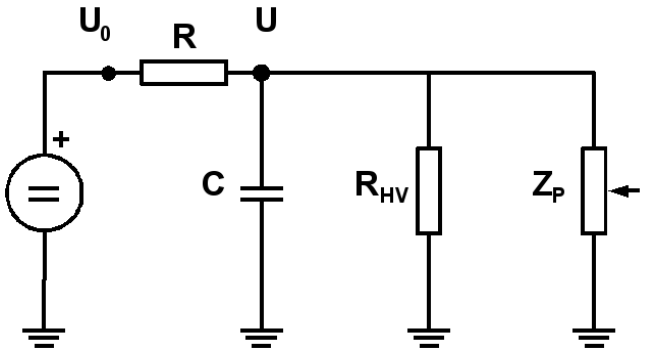

Figure 38. A simplified electric circuit representation of TS.

Figure 38 shows a simplified electric circuit representing TS. Here, C represents a sum of capacity of the HV cable (C_{cable}) connecting the resistor R (~10 MΩ) with the HV electrode, plus the internal capacity of the electrodes (C_{int}), plus the capacity of the HV probe (C_{probe} = 3 pF). If the length of the cable exceeds ~30 cm, C_{cable} dominates in C. The utilization of the HV probe also introduces a resistance R_{HV} = 100 MΩ, through which a parasitic loss current passes. Plasma is represented by an impedance Z_p. The unknown time-variable Z_p does not allow us to calculate the discharge current from the known value of U_0. However, accurate simultaneous measurements of both U_0 and U allow us to derive the relationship for the discharge current I:

$$I(t) = \frac{U_0(t) - U(t)}{R} - C\frac{dU}{dt} - \frac{U(t)}{R_{HV}} \tag{13}$$

This approximation is sufficiently accurate if $Z_p \approx R_p$ and the internal capacity of plasma is small compared to C. Under these assumptions, we can derive the changes of plasma resistance R_p from the calculated $I(t)$. This in turn enables us to calculate n_e in the plasma from its conductivity σ, which is related to R_p and n_e by equations

$$\sigma = \frac{n_e e^2}{m_e \nu} \tag{14}$$

$$\sigma = \frac{1}{\rho} = \frac{l}{S R_p} \tag{15}$$

where m_e is the electron mass, ν is the collision frequency of electrons with neutrals and l is the length of the plasma channel. From (14) and (15) we finally get:

$$n_e = \frac{l m_e \nu}{S R_p e^2} \tag{16}$$

Now we have obtained two different formulae to calculate n_e (equations 12 and 16). In both cases, the cross-sectional area S and the length l of the discharge channel should be measured by optical spectroscopic methods. We still have to know the value of either v_d or ν. Both these parameters are functions of E/N (Figure 39 and Figure 40) and can be calculated from the electron energy distribution function (EEDF). The collision frequency also depends on T_g (Figure 40) which can be measured from the emission spectra. To calculate EEDFs in air, we used the package Web-EEDF developed previously in our group [20], based on Monte Carlo simulations of electron dynamics.

As we assume that both formulae for the calculation of n_e are correct, we can link them to get a condition for v_d and ν:

$$v_d \times \nu = \frac{e\,U}{m_e\,l} \approx 3.5\times10^{18}\,U \quad [cm.s^{-2}] \tag{17}$$

Thus the product of these two unknown parameters is linearly proportional to the measured discharge voltage. Knowing the length of the discharge channel and T_g, and we can subsequently derive E/N for which this formula is valid.

Before applying all these formulae on TS, we should test them on the unstable glow regime (Figure 26c). Conditions during this unstable glow regime, such as average current or T_g, are closer to TS than conditions in the stable glow discharge. On the other hand, we can easily estimate the value of E/N in the positive column of this unstable glow regime and to compare this value with the value we get from (17).

Figure 41 shows the electric parameters of the unstable glow discharge regime with U_o = 9.2 kV (applied voltage), $U \approx 2.5$ kV (discharge voltage), and $I \approx 0.55$ mA. This I is much lower than in the stable glow regime (typically I >2 mA). This is due to the much higher value of the external resistor R here (11.5 MΩ). Therefore, the temperature inside the TS discharge channel is also lower: $T_g \approx 800$ K compared to 1900 K in the stable GD (see section 4.2.4). In this case we used a pin-to-pin configuration of stainless steel electrodes, where the cathode fall is near 269 V [15]. After subtracting this cathode fall, there remains around 2200 V for a 5 mm positive column, which gives $E/N \approx 75$ Td.

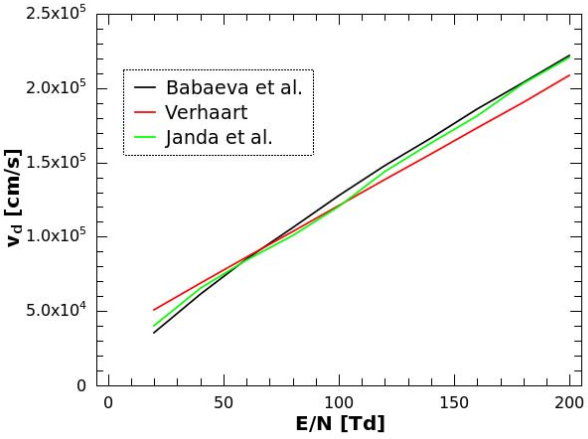

Figure 39. Drift velocity of electrons in air as a function of E/N, Verhaart [21], Babaeva et al. [22], Janda et al. [50].

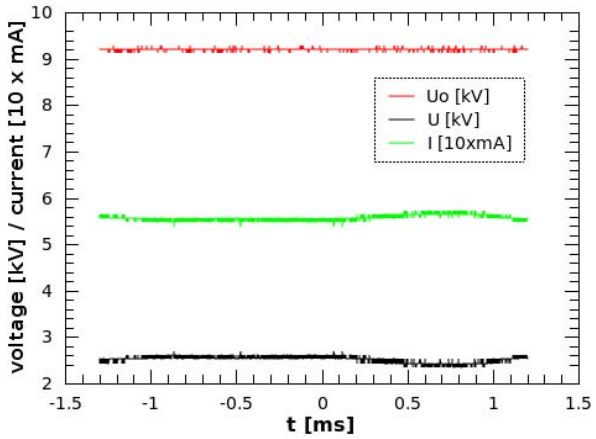

Figure 41. Measured electric parameters of the unstable glow regime.

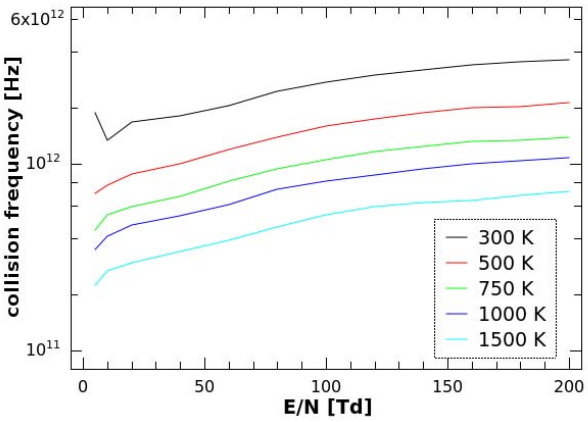

Figure 40. Collision frequency of electrons with neutrals in air as a function of E/N and T_g.

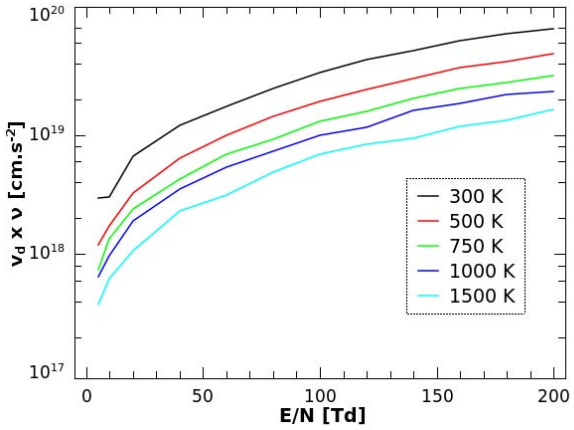

Figure 42. Product of $v_d \times \nu$ as a function of E/N and T_g.

According to (17), the product $v_d \times \nu \approx 8.8\times10^{18}$ cm.s^{-2}, which can be at ~800 K achieved only for $E/N \approx 70$ Td (Figure 42). This 70 Td is in a good agreement with the previously estimated 75 Td from the potential across the positive column. For $E/N = 70$ Td, both formulae (12) and (16) give n_e ~2×10^{11} cm^{-3}, using $S = 2\times10^{-3}$ cm^2 and $l = 0.5$ cm. Here we used the same S as for the stable glow discharge, though this approximation might not be perfectly correct.

The problem is that we cannot measure the diameter of the discharge channel of the unstable glow regime directly. The integrated emission measured by our Ocean Optics spectrometer always comprises many TS pulses, as well as unstable glow regime periods. Individual TS pulses create plasma channels in variable positions, thus leading to the enlarged volume from which the integrated emission can be measured. On the other hand, measurements with ICCD camera enable to make images of individual TS pulses, when triggered by themselves. Obviously, this method cannot be applied to the pulse-less GD. For TS pulses, ICCD imaging enabled us to estimate the channel diameter to around 0.2 mm (S ~ 4x10^{-4} cm^2), i.e. approximately twice less than the diameter of the stable GD with $I = 5$ mA (see section 4.2.4).

Now, we apply equations (12) to (17) on the TS pulse. Figure 43 shows the measured U waveform and the calculated I (in log scale). The capacity of the whole discharge system setup (cable, electrodes, HV probe) was found to be 27 pF to fit the measured current maximum. The

external resistor was 7.1 MΩ, and T_g around 600 K, the HV cable length ~65 cm (unlike 10 MΩ and ~30 cm cable used previously and analyzed in section 4.4.1).

Despite having measured the temperature from the time-integrated spectra, we suppose that it well represents the temperature during the period shown in Figure 43. The reason is that according to the time-resolved ICCD measurements, almost entire emission of the N_2 second positive system occurs within 20 ns after the beginning of the current pulse, as described in section 4.4.3. The 20 ns period is too short for vibrational-translational (VT) transfer mechanism of the gas heating, for its characteristic time is in order of microseconds. Therefore, the measured temperature is elevated from the ambient one due to the previous TS pulses. The TS T_g is given by equilibrium between the discharge heating and the energy dissipation between the pulses.

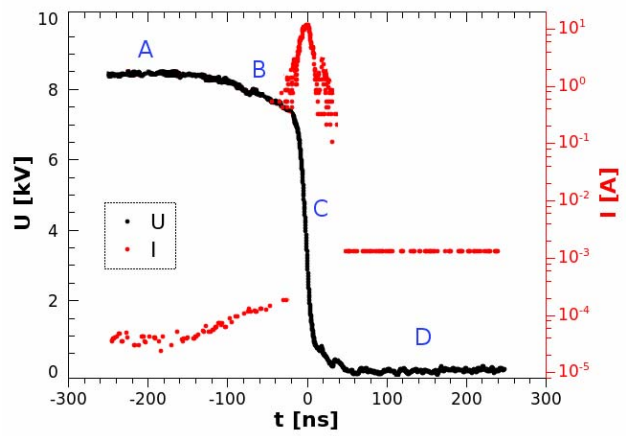

Figure 43. Measured voltage and calculated current of a TS pulse.

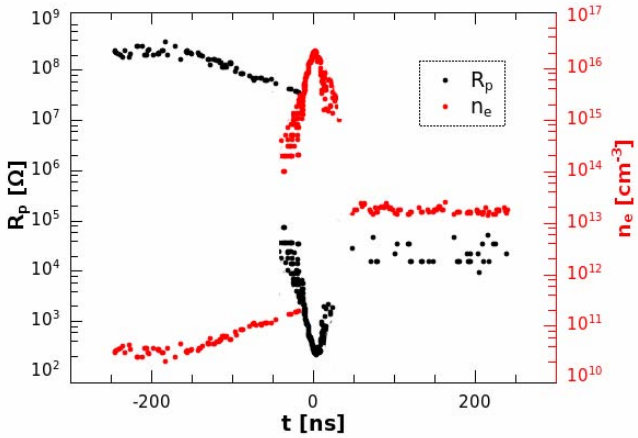

Figure 44. Calculated concentration of electrons and plasma impedance during a TS pulse.

As the next step, we calculated $v_d \times \nu$ from the measured voltage (equation 17). For U_{max} ~ 8.5 kV this gives a value ~3×10^{19} cm.s^{-2}, which can be obtained for E/N ~ 150 Td at 600 K. From the calculated values of E/N we get values of v_d, which can be then used to calculate n_e. However, as previously mentioned, the situation in TS is more complicated than in GD because E/N is a function of time and position in the reactor. For this reason, we discuss the validity of the results presented in Figure 44 by dividing the whole TS period into four segments representing different steps in the evolution of the TS pulse. These time segments are depicted in Figure 43 by letters A, B, C, and D and their boundaries are well defined by the changes in the current value and its trend.

A.) This region represents the streamer corona discharge regime with the current of tens of μA. It is also the weakest point of our calculation. The electric field in pin-to-pin electrode configuration of can be approximated by a strongly non-homogeneous Laplacian field. There are two ionization regions with strong field near the tips of the electrodes, and a drift region in the central part of the discharge gap. In the ionization regions, the drift velocity is high, but the cross-sectional area of the discharge is small. On the other hand, in the drift region, the area is larger but the drift velocity is smaller. Since n_e depends on the product of S and v_d (equation 12), these two effects partially compensate each other and n_e should be more evenly distributed along the axis connecting the tips of the electrodes than E/N. Our calculation based on (17) gives E/N ~ 150 Td. However, it is based on the approximation by the cross-sectional discharge column area S ~ 4×10^{-4} cm^2 that may not be accurate for corona. We should in fact use some

larger area, leading to the smaller n_e. Therefore, the calculated E/N ~ 150 Td is only an average (effective) value. E/N is probably stronger near the tips, whereas in the drift region, it is certainly below 120 Td (breakdown value in air). Finally, we emphasize that the calculated $n_e \sim 10^{10}$ cm^{-3} is only an average or characteristic value for A region.

B.) Streamer corona eventually leads to the formation of a streamer which bridges the whole discharge gap and creates a conductive channel. In the first moment, the conductivity of this channel is still quite week, i.e. the impedance of the plasma gap still remains high (Figure 44) and the charge stored in the internal capacity C can be only slowly discharged through this channel.

We assume that the plasma region can be better approximated by a column during this period B, although its S is still questionable. We suppose it should be only slightly smaller than the area of the later high current pulse. The applied voltage is still high (~ 8 kV), so if the E/N is constant, it should be around 130 – 140 Td (16 kV/cm at 600 K). We suppose that E/N is still similar to Laplacian field with larger values near the electrode tips but with the smaller difference between the field in the middle and near the tips than in corona. This transition to TS pulse probably starts when E/N in the middle of the gap surmounts the breakdown value of 120 Td and this is already close to that average value of maximum 140 Td. Strong filed all across the gap results in the growth of n_e from 10^{10} to 10^{11} cm^{-3} in the whole plasma channel thanks to the electron impact ionization processes. This growth causes the decrease of R_p and enables faster discharging of C.

C.) A positive feedback – more charge from C means higher n_e and smaller R_p - leads to the acceleration of this process and the formation of the high current TS pulse. On the other hand, this is accompanied by the decrease of U_0, thus making the electron impact ionization no more effective in the plasma column. During this period, TS represents a short arc with thin cathode and anode layers and relatively long and homogeneous plasma column with low E/N. So, our approximation by a column with $S \sim 4\times10^{-4}$ cm^2 is accurate during this period. On the contrary, the voltage drops from ~8 kV to only a few tens of volts here and this is too small to be correctly measured with the HV probe. Therefore, there is an uncertainty concerning the value of E/N and thus also v_d. The n_e achieves a maximum of 10^{16} cm^{-3}.

D.) As soon as C is completely discharged, I and n_e drop quickly. The plasma channel still remains there, although its impedance increases to more than 10 kΩ. I is now limited by the value of external resistance R. In this case it leads to I ~ 1 mA. Thus, this period can be considered as a short glow discharge period. We can therefore approximate this period by a plasma column as well. Its area should perhaps increase with time, although just slightly during the period shown in Figure 43 and Figure 44. Again, the accuracy of calculated $n_e \sim 10^{13}$ cm^{-3} is affected by the questionable estimate of E/N due to the inaccurate measurement of U.

We have discussed the problems with calculation of n_e in TS. Finally we found that the period after the high current pulse is similar to the GD discharge regime with the current around 1 mA and $n_e > 10^{13}$ cm^{-3}. To check whether we can calculate n_e in this after-pulse period, we applied the same procedure of estimation of v_d, effective E/N and n_e from longer voltage waveforms including more TS pulses and a transition into the unstable glow regime (Figure 45). This estimation of n_e (Figure 46) is just very rough for the period long after the TS current pulse, assuming a constant $S \sim 4\times10^{-4}$ cm^2. This output will be checked in the future. We will attempt to find a discharge regime optimized to keep n_e always above 10^{12} cm $^{-3}$.

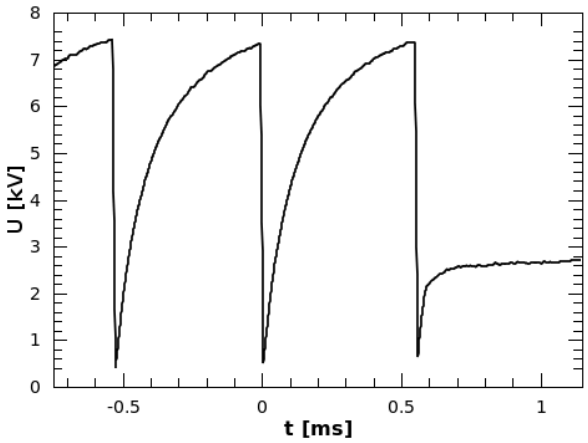

Figure 45. Measured voltage waveform of several TS pulses.

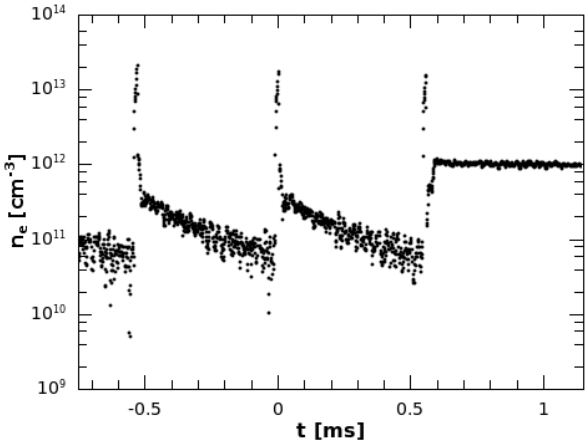

Figure 46. Calculated concentration of electrons for several TS pulses.

5. Conclusions and Perspectives

This final report summarizes the progress of the current program to investigate the volume scalability and power reduction of nonequilibrium plasmas produced by electrical discharges in atmospheric pressure air, as well as to investigate related fundamental phenomena. Key results to date demonstrate that both DC glow discharge and pulsed transient spark generate air plasmas of required parameters.

The experiments with DC glow discharge in ambient and preheated air provide basic characteristics of these nonequilibrium atmospheric pressure air plasmas. DC Glow discharge is easier for volume scaling but requires larger power, 3-60 W. It produces stable nonequilibrium air plasma with gas temperatures of 1500-2500 K and electron densities ~10^{12} cm^{-3}. Electrical measurements and optical emission spectroscopy confirmed that this pulse-less discharge regime is glow and not arc. GD operated in preheated air improves the volume scaling but at very high powers (including the preheating). We emphasize the mechanism of gas heating via vibrational-translational (V-T) energy transfer because it is found to influence the discharge properties and volume considerably. Corona as a temperature probe was developed to diagnose the microwave preheated air.

A new concept of the DC-driven pulsed discharge was tested: transient spark, a repetitive streamer-to-spark transition discharge regime of very short pulse duration (~10-100 ns) and with a very limited energy so that the generated plasma is highly nonequilibrium. This discharge can be maintained at low energy conditions by an appropriate choice of the resistances and capacities in the electrical circuit, and its frequency can be controlled by the applied voltage. Its activity is comparable with the nanosecond repetitive pulsed discharges but its advantage is an easy DC operation and no need of special and expensive high voltage pulsers with high repetitive frequencies and nanosecond rise-times. Its typical power budget is 0.1-2 W, lower than with glow discharges. Detailed electrical characteristics were given. The preliminary results on nanosecond time scale discharge evolution seem very interesting with many questions still open. We estimated the time evolution of the electron density before, during and after the TS pulse.

In the next period (in the following EOARD project) we plan further investigations of the temporal evolution of processes occurring in TS via ICCD highly temporally and spectrally resolved optical emission spectroscopy combined with electrical measurements. A comprehensive analysis of the obtained results, as indicated by the preliminary tests, will expectantly lead to for deeper understanding of the elementary processes occurring in these repetitive pulses. The problem of ICCD triggering without losing the first 20 ns of the pulse must be resolved. The optimum TS conditions with n_e kept abobe ~10^{12} cm^{-3} at all times will be sought.

We also plan further experiments with GD, as well as TS in preheated air. We also envisage testing the GD properties at reduced pressures and comparing the effect of reduced pressure with the elevated temperature.

In summary, atmospheric pressure air plasmas generated by the glow discharge and transient spark represent a potential for aircraft shielding, and many other applications.

6. Personnel

Comenius University, Faculty of Mathematics, Physics and Informatics:
Principal investigator: Prof. Zdenko Machala, PhD.
Vice-principal investigator: Prof. Karol Hensel, PhD.
Other personnel:
Mário Janda, PhD.
Igor Jedlovský, MSc., Lenka Leštinská, MSc. (PhD students)
Lenka Chládeková, Lukáš Dvonč, Jozef Síč, Michal Pelach (MSc and Bc students)

International collaboration:
Prof. Christophe O. Laux, PhD., Ecole Centrale Paris, France (consultant)
Dr. Emmanuel Marode, research director at CNRS, Univ. Paris XI, France (consultant)

7. Honors / Awards

-
- 2008 Zdenko Machala, Award of the Slovak Physical Society, 1^{st}-2^{nd} ranking in the Scientific competition of the young researchers
- 2008 Zdenko Machala, Honorable Award of the Journalist-Studio Bratislava within the awards "Scientist of the Slovak Republic of the year 2008"

8. Publications

Reviewed papers:

1. Z. Machala, I. Jedlovský, V. Martišovitš: *DC discharges in atmospheric air and their transitions,* IEEE Trans. Plasma Sci. **36** (2008) 918-919
2. L. Leštinská, V. Martišovitš, M. Zahoran, Z. Machala: A*tmospheric pressure microwave plasma for waste carbon treatment*, Chem. Listy **102** (2008) s1428-1431
3. Z. Machala, I. Jedlovský, L. Chládeková, B. Pongrác, D. Giertl, L. Šikurová: *DC discharges in atmospheric air for bio-decontamination – spectroscopic methods for mechanism identification,* Eur. J. Phys. D **47** (2009) 195-204
4. Z. Machala: *Bio-decontamination by DC corona and transient spark in atmospheric air: microbial inactivation mechanisms,* Plasma Sources Sci. Technol. (2009) submitted

Conference contributions:

Invited:

1. Z. Machala, Bio-decontamination by DC discharges at atmospheric pressure: identification of microbial inactivation mechanisms, invited topical lecture, 29th Int. Conf. Phenomena Ionized Gases, 12-19 July 2009, Cancun, Mexico

Regular:

2. L. Leštinská, Z. Machala: *Corona discharge as a diagnostic probe for temperature measurements of atmospheric microwave plasma*, 19th Int. Symp. Plasma Chemistry, 26-31 July 2009, Bochum, Germany
3. Z. Machala, I. Jedlovský, B. Pongrác, L. Chládeková, D. Giertl, L. Šikurová: *Various DC discharges for sterilization at atmospheric pressure,* 11th Int. Symp. High Pres. Low Temp. Plasma Chemistry HAKONE XI, Oleron, France, 7-12 September 2008, p. 530-534
4. M. Janda, Z. Machala, D. Pai, G.D. Stancu, D. Lacoste, C.O. Laux: *Transient spark discharge in air*, 11th Int. Symp. High Pres. Low Temp. Plasma Chemistry HAKONE XI, Oleron, France, 7-12 September 2008, p. 85-89
5. Z. Machala, I. Jedlovský, D. Giertl, L. Chládeková, B. Pongrác, M. Zvarík, L. Šikurová: *Sterilization by DC discharges at atmospheric pressure*, 23rd Symposium Plasma Physics Technol., Prague, Czech Rep., June 2008, p. 130
6. M. Janda, Z. Machala, M. Morvová: *Transient spark in N2/CO2/H2O mixtures at atmospheric pressure*, 23rd Symposium Plasma Physics Technol., Prague, Czech Rep., June 2008, p. 98-99

9. References

[1] *Mechanisms of Ionizational Nonequilibrium in Air Plasmas,* Final Technical MURI Report, submitted to AFOSR by C.H. Kruger, October 2002

[2] *Scaled-up Nonequilibrium Air Plasmas,* Final Technical Report, submitted to AFOSR by C.H. Kruger, C.O. Laux, Z. Machala, and G.V. Candler, January 2004

[3] C. O. Laux: *Radiation and Nonequilibrium Collisional-Radiative models,* von Karman Institute for Fluid Dynamics, Lecture Series 2002-07, Rhode Saint-Genese, Belgium, June 2002; *www.**specair**-radiation.net*

[4] U. Fantz: Plasma Sources Sci. Technol. **15** (2006) S137–S147

[5] Z. Machala, M. Janda, K. Hensel, I. Jedlovský, L. Leštinská, V. Foltin, V. Martišovitš, M. Morvová: J. Mol. Spectrosc. **243** (2007) 194-201

[6] C. O. Laux, T.G. Spence, C.H. Kruger, R.N. Zare: Plasma Sources Sci. Technol. **12** (2003) 125-138

[7] R. S. Sigmond: J. Appl. Phys. **56**, 1355–1370 (1984)

[8] E. Marode, F. Bastien, M. Bakker: J. Appl. Phys. **50**, 140-146 (1979)

[9] G. V. Naidis: J. Phys. D: Appl. Phys. **38** 3889–3893 (2005)

[10] Z. Machala, C.O. Laux, X. Duten, D.M. Packan, L. Yu, C.H. Kruger: *Scaled-up Nonequilibrium Air Plasmas,* 41st Aerospace Sciences Meeting and Exhibit, Reno, NV, USA, 6-9 January 2003, AIAA 2003-874

[11] Z. Machala, C.O. Laux, C.H. Kruger and G.V. Candler: *Atmospheric Pressure Air and Nitrogen DC Glow Discharges with Thermionic Cathodes,* 42nd Aerospace Sciences Meeting and Exhibit, Reno, NV, USA, 5-8 January 2004, AIAA 2004-355

[12] Z. Machala, E. Marode, C.O. Laux, C.H. Kruger: J. Advanced Oxid. Technol. **7** (2004) 133-137

[13] L. Yu, C. O. Laux, D. M. Packan, and C. H. Kruger: J. Appl. Phys. **91**, 2678-2686, (2002)

[14] C. H. Kruger, C. O. Laux, L. Yu, D. M. Packan, and L. Pierrot: Pure and Applied Chemistry **74** (2002) 337-347

[15] Yu. P. Raizer: *Gas Discharge Physics,* New York: Springer (1991)

[16] A. P. Yalin, R. N. Zare, C. O. Laux, and C. H. Kruger: Appl. Phys. Lett. **81** (2002) 1408-1410

[17] Z. Machala: *Continuous and transient electrical discharges, streamer triggered, at atmospheric pressure, for the removal of Volatile Organic Compounds (VOC),* PhD. thesis, University Paris-Sud XI, France, Comenius University Bratislava, Slovakia, 2000

[18] Z. Machala, M. Morvová, E. Marode, I. Morva: J. Phys. D: Appl. Phys. **33** (2000) 3198-3213

[19] Z. Machala, I. Jedlovský, V. Martišovitš: IEEE Trans. Plasma Sci. **36** (2008) 918-919

[20] M. Janda et al.: Acta Phys. Slovaca **55** (2005) 507–514

[21] H. F. A. Verhaart: Kema Scient. Tech. Rep. **7** (1989) 377

[22] N. Yu. Babaeva et al.: *The Streamer Propagation Models in N2-O2 Mixtures and Flue Gas,* Research Report IVTAN ANRA 93/2, Moscow (1993)